AlGaN/GaN HEMT DC Simulation

by

Ruocan Wang

A thesis submitted to the Graduate Faculty of
Auburn University
in partial fulfillment of the
requirements for the Degree of
Master of Science

Auburn, Alabama
May 3, 2014

Keywords: GaN HEMT, TCAD simulation, high power devices

Approved by

Guofu Niu, Professor of Electrical and Computer Engineering
Fa Dai, Professor of Electrical and Computer Engineering
Bogdan Wilamowski, Professor of Electrical and Computer Engineering
Minseo Park, Professor of Physics

Abstract

Increasing demand in high power and high frequency semiconductor devices has promoted the rapid development of microwave power devices using GaN and SiC. Characteristics like high breakdown voltage and high electron mobility enable AlGaN/GaN HEMT the possibility to be utilized as high power RF devices. However, obstacles prevent the widely utilization of AlGaN/GaN transistor in this field. It has been generally recognized the superabundant trap density in GaN and AlGaN material limits the performance of the devices by bringing in reliability issues like current collapse and gate-lag. Lattice mismatch in GaN and AlGaN and abrupt heterojunction interface of AlGaN/GaN contribute to the unstable performance while high voltage is applied to drain contact which will cause high field between thin layer of AlGaN/GaN interface.

An overall introduction to HEMT physics will be presented in chapter 2 of this work. Attention will be paid to the performance degradation analysis caused by issues such as trapping effect, self-heating, displacement damage and high voltage induced lattice mismatch.

The chapter 3 of this work presents a process to use TCAD simulation tool to match the simulation results with measurements from real devices starting from building device structure. Adjustments of parameters including gate barrier height, electron mobility, polarization coefficients and parasitic resistance will be made to fit the measurements.

Acknowledgments

I would like to express thanks to my professor Dr. Guofu Niu for giving me the opportunity to finish my master's thesis. I would like to thank Dr. Niu for the continuous patience, encouragement and academic support he offers during my master's program study.

I am grateful for my group members for all the help they provide, and kindly accompany through the long, tough but meaningful years of study in Auburn. I would like to express thanks to Dr. Park and his students Fei and Henry for their support in device measurement.

Last but not the least, I would like to express my gratefulness to my parents for their love, patience, encouragement and support since I was born. Without them, I will not be able to get so far.

Table of Contents

List of Figures

List of Tables

Chapter 1

Introduction

Recent progress in research of wide band gap material has been successful in attracting attention in application of wide band gap material in device fabrication during the last 10 years. Compared to the most popular semiconductor materials, the majority of the WBG (wide band gap) material utilizations are in optoelectronics such as shortwave light emitting diode and high power electronic devices. Another application of WBG material is RF device that requires rapid carrier transport which results from the formation of two dimensional electron gas due to polarization effect [1].

This thesis consists of four chapters. The first chapter presents the motivation and outline of this work. A brief background introduction is presented in Chapter 2 including wide band gap material properties, polar material, polarization effect and mechanism of GaN HEMT. Simulation is illustrated in Chapter 3 consisting of building structure, specifying parameters, fitting measurement and gate scaling. Fitting of measurement and gate scaling are applied to $I_d - V_d$ and $I_d - V_g$ curves.

Chapter 2

Background

In this chapter, a brief introduction of WBG material characteristics is presented in the first and second sections for the goal of further discussion of HEMT models mentioned in Chapter 3. Most of the attention is drawn on GaN and AlGaN, which are the predominant materials used to fabricate HEMT this thesis concerns.

2.1 Brief introduction of wide band gap (WBG) material

The predominant advantage of wide band gap materials over other semiconductors is large band gap energy E_g which enables their application in high power devices where high electric breakdown field is required. Table 2.1 reports material properties of AlN, SiC, GaN, GaAs and Si including band gap, electric breakdown field, saturated electron velocity, electron mobility, lattice constant and so on.

Intrinsic carrier concentration increases along with temperature. When the intrinsic carrier concentration increases above $10^{15} cm^{-3}$, the material is unsuitable for electronic devices [1]. Compared with other semiconductors like Si, intrinsic concentration of wide band gap material is lower under same temperature which offers WBG material the potential to operate under high temperature. Figure 2.1 shows intrinsic carrier concentrations of several semiconductors respect to temperature. GaN intrinsic carrier concentration at 300K is below $10^4 cm^{-3}$ which is several orders of magnitude smaller than that of Si.

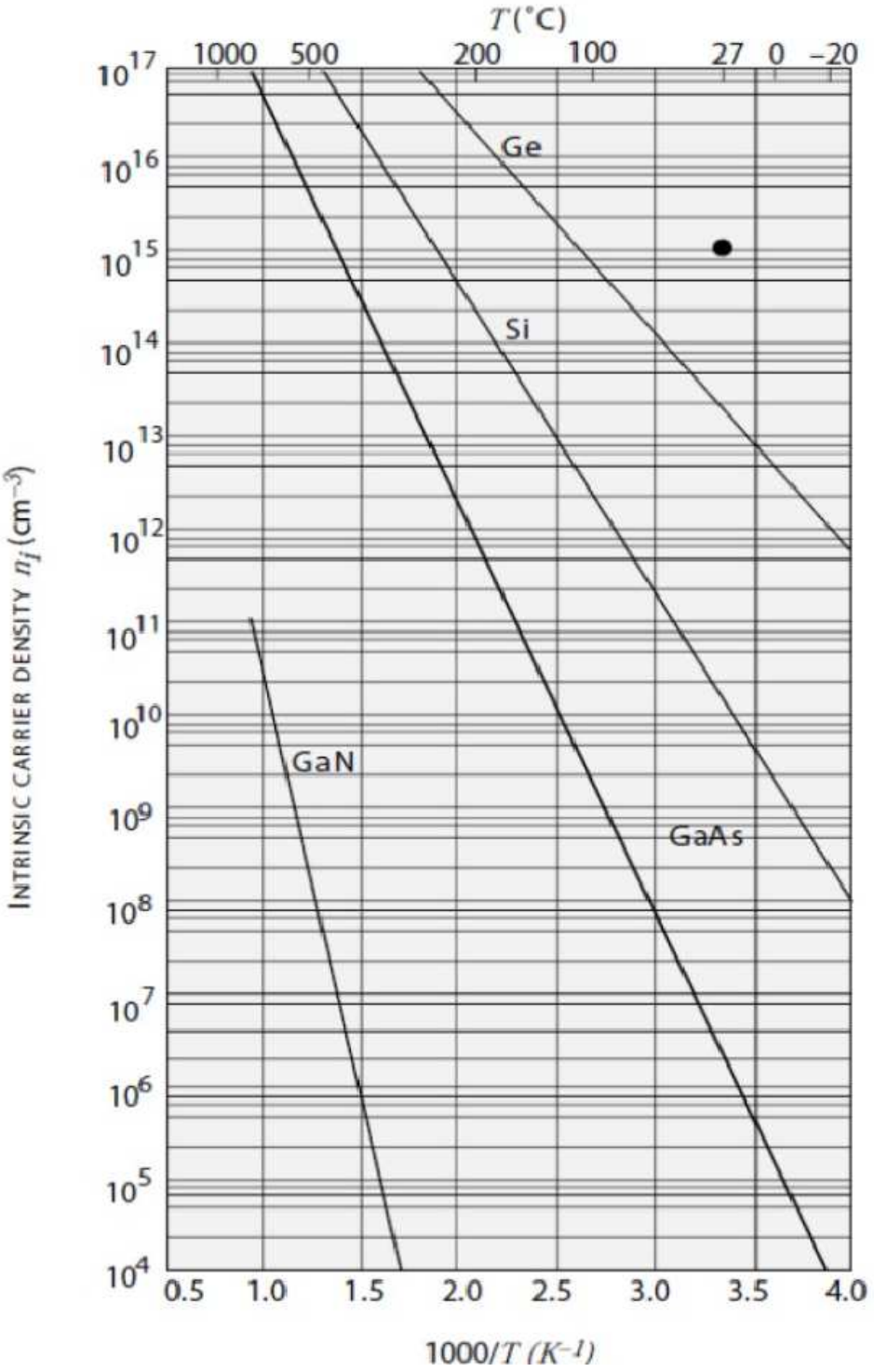

Figure 2.1: Intrinsic electron concentration of Si, Ge, GaN and GaAs respect to temperature [1].

Property	GaN	AlN	InN	SiC	Si	GaAs
Band Gap (E_g) $[eV]$	3.44	6.2	1	3.26	1.12	1.43
Electric breakdown field (E_c) $[MV/cm]$	3.0	1.4-1.8	3.0	3.0	0.4	0.5
Saturated electron velocity (v_{sat})$[10^7 cm/s]$	2.5	1.7	4.5	2.0	1.0	1.0
Electron mobility (μ_n)$[cm^2/V \cdot s^{-1}]$	2000	135	3200	700	1500	8500
Electron effective mass (m_c)$[m_0\ ]$	0.22	0.44	0.11	0.2	1.18	0.63
Electron effective mass (m_v)$[m_0\ ]$	0.8	3.53	0.27	1.0	0.55	0.52
Lattice constant	3.175	3.11	3.533	3.073	5.431	5.653

Table 2.1: Properties of various semiconductors [1].

2.2 Material properties

2.2.1 GaN(gallium nitride)

In the HEMT studied in this thesis , GaN is used to construct the bulk region and channel region considering its electric properties. It is also a dominant material compositing HEMT channel and buffer in commercial HEMT fabrication where fast carrier transport and high breakdown voltage are desired. Moreover, WBG materials have large saturation velocity which allows them to operate under high electric field. Although reported outstanding characteristics make WBG materials suitable for working under high electric field, WBG materials still have disadvantages that cannot be ignored. Compared with conventional semiconductor material for example GaAs, relatively low electron mobility in bulk GaN is the main shortage in fabricating HEMT. The bulk GaN electron mobility is about 800 - 900 $cm^2/V \cdot s^{-1}$ which is one order lower in magnitude than GaAs which has mobility of 8500 $cm^2/V \cdot s^{-1}$.

Though low in intrinsic material electron mobility, the electron mobility in heterojunction interface of AlGaN/GaN is high enough to achieve good performance. At the heterojunction interface between GaN and AlGaN, a relatively high electron concentration can

Property	GaN	AlN	InN	SiC	Si	GaAs
Thermal conductivity(κ)$[W/cm \cdot K]$	1.3-2.1	2.85	0.45	3.7-4.5	1.5	0.5

Table 2.2: Thermal conductivity of various semiconductors.

be achieved as a result of polarization effect even without intentional doping. The high concentration electron at the interface due to polarization effect is called two-dimensional-electron-gas (2DEG). This sheet of electron locates at the top of GaN layer which is channel of HEMT provides path for current flowing from drain to source. Electron mobility in channel region is reported to be between 1200 $cm^2/V \cdot s^{-1}$ to 2000 $cm^2/V \cdot s^{-1}$ which is higher than that in the bulk region of which electron mobility is reported to be 800 $cm^2/V \cdot s^{-1}$ [1].

Another advantage of WBG materials over conventional semiconductors is their large thermal conductivity (κ). High thermal conductivity is essential to the high temperature performance of a device. Thermal conductivity reveals the ability of a material to extract dissipated power away from the device which further enables device operation under high temperature. Table 2.2 shows thermal conductivities of several semiconductors at 300K including WBG materials and conventional semiconductors such as Si and GaAs. Conventional semiconductors, particularly GaAs has poor thermal conductivity of 0.5 $W/cm \cdot K$. On the contrary, WBG materials, for instance, SiC and AlN are excellent in power extracting with high thermal conductivities of 3.7-4.5 $W/cm \cdot K$ and 2.85 $W/cm \cdot K$ respectively.

Thermal conductivity of GaN is reported to be $1.7 W/cm \cdot K$ by Slack [2]. However, in reality, the measured thermal conductivity of GaN reveals a peak value of 1.3 $W/cm \cdot K$ which is slight lower than that reported by Slack. Research in this field indicates that the effects of impurities and dislocations are responsible for the decrement of thermal conductivity. The lattice constant of SiC and GaN are quite similar, therefore SiC can be used as substrate for Si to grow on since utilizing of high thermal conductivity of SiC will enable device cooling off effectively.

2.2.2 AlN (aluminum nitride) and AlGaN (aluminum gallium nitride)

Being one of the most important binary material in III-V material family, AlN is an insulator with a band gap of $6.2eV$ which is difficult for electron in valence band to be excited. AlN can be used as nucleation layer between SiC or sapphire substrates and bulk GaN since intrinsic AlN has high thermal conductivity which will help dissipated heat to be removed from device [3]. Additionally, nucleation layer can modify the breakdown voltage of GaN buffer layer. Young Chul Choi's paper [3] shows the thickness of AlN nucleation layer has dominant influence on the breakdown voltage of devices.

Ternary compound of AlN such as AlGaN is widely used in heterojunction of HEMT. Highly doped AlGaN is source of electron in GaN channel in devices where AlGaN is used as barrier layer on top of GaN. Equation (2.1) shows the calculation of model parameters of ternary compound AlGaN using corresponding parameters of AlN and GaN.

$$P_{A_xB_{1-x}N} = x \cdot P_{AN} + (1-x) \cdot P_{BN} \tag{2.1}$$

In Equation (2.1), $P_{A_xB_{1-x}N}$ stands for a certain parameter of $A_xB_{1-x}N$ that needs to be calculated from the corresponding ones of binary compound AN and BN. Parameters of AlN and GaN include spontaneous polarization, elastic constants, piezoelectric coefficients which will determine the calculation of polarization charge density and 2DEG density. Calculation of charge densities will be illustrated in the next subsection.

2.3 Polar material and polarization effect

Three crystal structures exist in Nitride compounds: wurtzite, rock-salt and zinc-blende. In electronic devices, Wurtzite crystal material is prevalently used. Its crystal structure is called the wurtzite crystal structure which is a member of the hexagonal crystal system

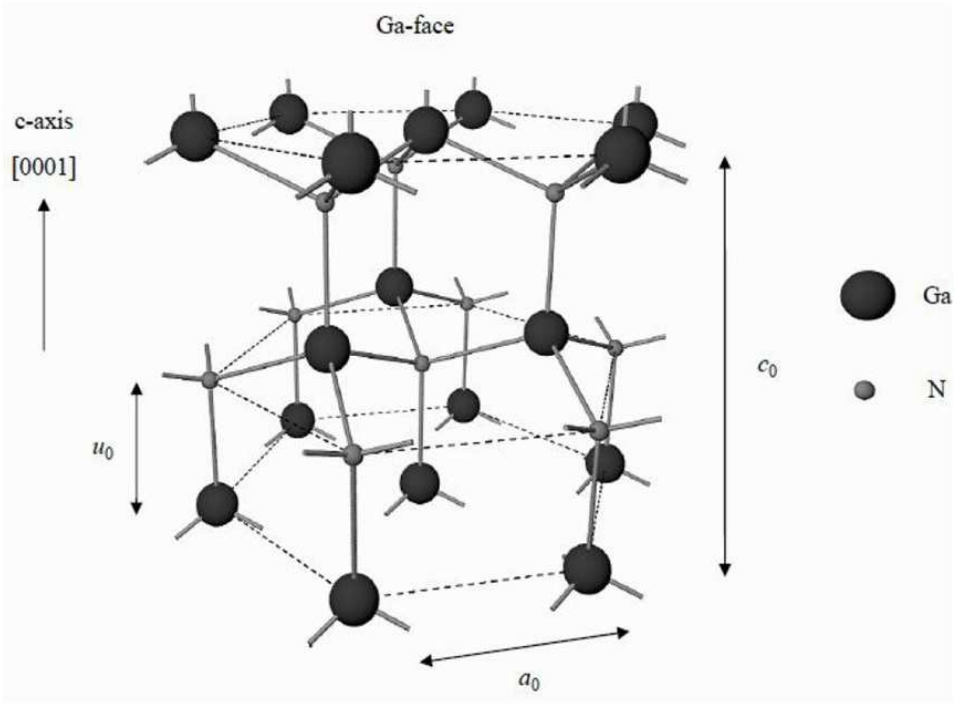

Figure 2.2: Crystal structure of Ga face GaN [1].

and consisting of tetrahedrally coordinated zinc and sulfur atoms that are stacked in an ABBABBABB pattern.

Figure 2.2 shows the crystal structure of Ga-face GaN. In GaN material, as shown in Figure 2.2, each Ga atom is bonded by the other four adjacent N atoms while each N atom is bonded by other four adjacent Ga atoms as well. The solid line represents the chemical bond between atoms and dash line is used to indicate that atoms are in the same plane. The wurtzite crystal structure then can be departed into identical segments that periodically repeat in space domain. The horizontal direction is parallel to the plane of GaN growth. The vertical direction is along the direction that GaN grows.

It can be observed that the wurtzite crystal structure is not central symmetric along the vertical direction which is called c-axis [0001]. Net volume dipole moment is nonzero in the nitride crystal even when no external electric field is applied to the structure. The polarization effect caused by non-central-symmetric structure in GaN is called spontaneous

polarization effect. Spontaneous polarization effect also exists in AlGaN, which is different in magnitude from that of GaN. The difference of spontaneous polarization of GaN and AlGaN is one source of 2DEG.

Depending on the kind of atom of the basal layer, GaN can be divided into Ga-face and N-face. In Ga-face GaN, Ga atoms consist the top layer along the direction of the growth and Ga-face GaN corresponds to [1000] polarity. Ga-face GaN and N-face GaN are different in chemical, physical and electrical properties. The spontaneous polarization for GaN and AlN is negative for layers grown in the [0001] direction and increases in magnitude by going from GaN to AlN [4]. Direction of polarization affects the sign and amount of polarization charge at heterojunction interface, which will further influence the sign and density of polarization induced charge and 2DEG. In this work, Ga-face GaN is used for simulation since most GaN is Ga-face by nature.

Piezoelectric polarization is a result of the strain or stress of the crystal lattice due to physical distortion while layers are connected at the heterojunction interface. Due to the differences in the lattice constants of AlN, GaN and AlGaN, growing AlGaN on GaN leads to compressive strain in AlGaN [14]. A few other papers reports in detail the direction of polarization in different combination of materials [9], [10].

At an abrupt interface, the polarization sheet charge density is defined as the difference in charge densities between the upper and lower layers. Equation (2.2) shows the way of calculation of charge density at the heterojunction interface due to spontaneous polarization and piezoelectric polarization.

$$\sigma = P(AlGaN) - P(GaN) = P_{SP}(AlGaN) + P_{PE}(AlGaN) - P_{SP}(GaN) \quad C/cm^2 \quad [1] \tag{2.2}$$

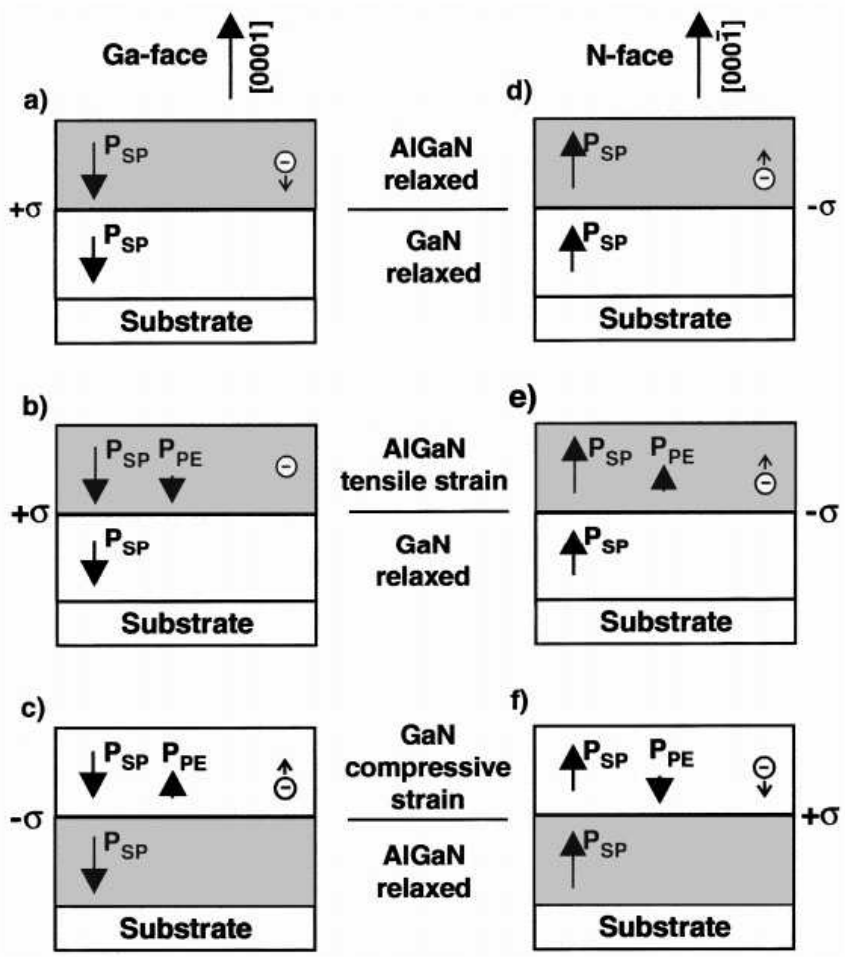

Figure 2.3: Polarization effect in Ga-face and N-face GaN [9].

$$P_{PE} = 2\frac{a - a_0}{a_0}(e_{31} - e_{33}\frac{C_{13}}{C_{33}}) \quad C/cm^2 \quad [1] \tag{2.3}$$

$$P_{SP}(x) = -0.052x - 0.029 \quad C/cm^2 \quad [1] \tag{2.4}$$

$$P_{SP}(0) = -0.029 \quad C/cm^2 \quad [1] \tag{2.5}$$

$$\sigma(x) = (2\frac{a - a_0}{a_0}(e_{31} - e_{33}\frac{C_{13}}{C_{33}}) + P_{SP}(x) + P_{SP}(0)) \times \frac{1}{e} \quad /cm^2 \quad [1] \tag{2.6}$$

Equation (2.3) shows the calculation of piezoelectric polarization using piezoelectric coefficients and elastic constants. In Equation (2.3), e_{33} and e_{31} are piezoelectric coefficients, C_{33} and C_{13} are elastic constants. Piezoelectric coefficient e_{33} and e_{31} are related to lattice constant a_0 and a_x. Equation (2.4) and (2.5) show the calculation of spontaneous polarization in AlGaN and GaN respectively which are dependent of Al mole composition x. Unit of piezoelectric coefficient and spontaneous coefficient is C/cm^2 while unit of elastic constants is Pa. Values of piezoelectric coefficient, elastic constants and spontaneous polarization are presented in comparison of charge placement methods in Chapter 3. The density of polarization induced charge is equal in amount to the sum of piezoelectric polarization charge and spontaneous polarization charge but negative in sign in order to maintain the charge neutrality in whole structure. Equation (2.6) shows the calculation of amount of polarization induced charge density. The first term in Equation (2.6) is equal to Equation (2.3) which

indicates the amount of piezoelectric polarization in AlGaN. The second term $P_{SP}(x)$ and third term $P_{SP}(0)$ indicate spontaneous polarization in AlGaN and GaN respectively. Values of piezoelectric coefficients, spontaneous coefficients and elastic constants used for simulation are provided in Chapter 3.

Figure 2.3 shows signs and locations of polarization induced charges in different heterojunction structures. In the case of Ga-face AlGaN/GaN heterojunction with AlGaN on the top, sum of polarization induced charge is positive which is shown in Figure 2.3 b). Free electrons will accumulate at the GaN top to compensate polarization induced charge to hold neutrality. These electrons will form a 2DEG with a sheet carrier concentration n_s by assuming that the AlGaN/GaN band offset is reasonably high and that the interface roughness is low.

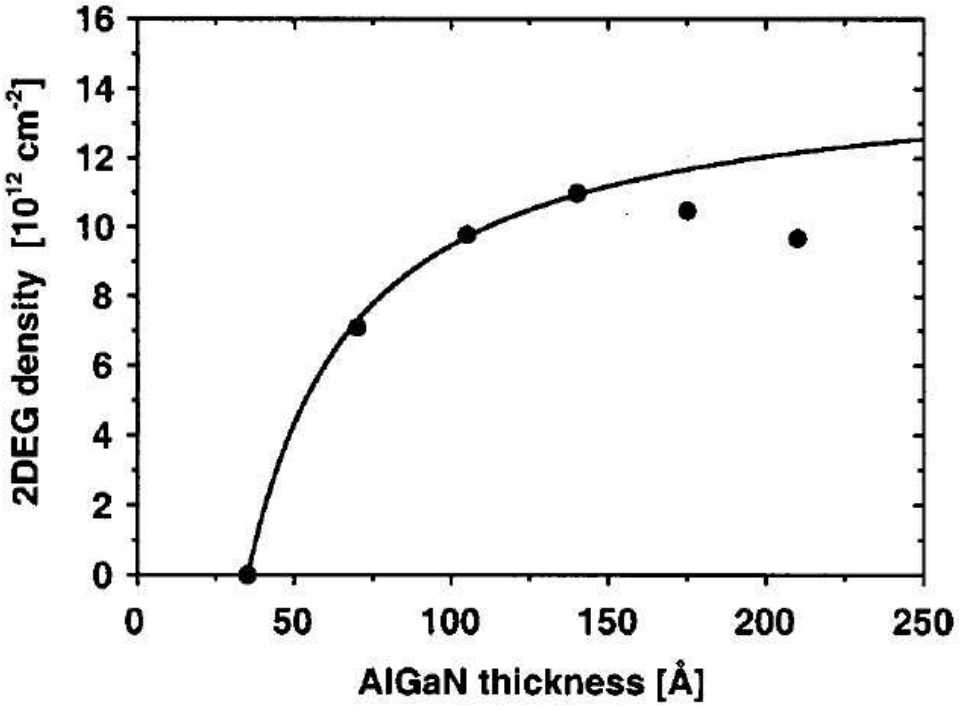

Figure 2.4: 2DEG sheet charge density as a function of AlGaN barrier thickness at room temperature from an AlGaN/GaN diode structure with Schottky contact on AlGaN and Ti Ohmic contact on GaN[4].

.

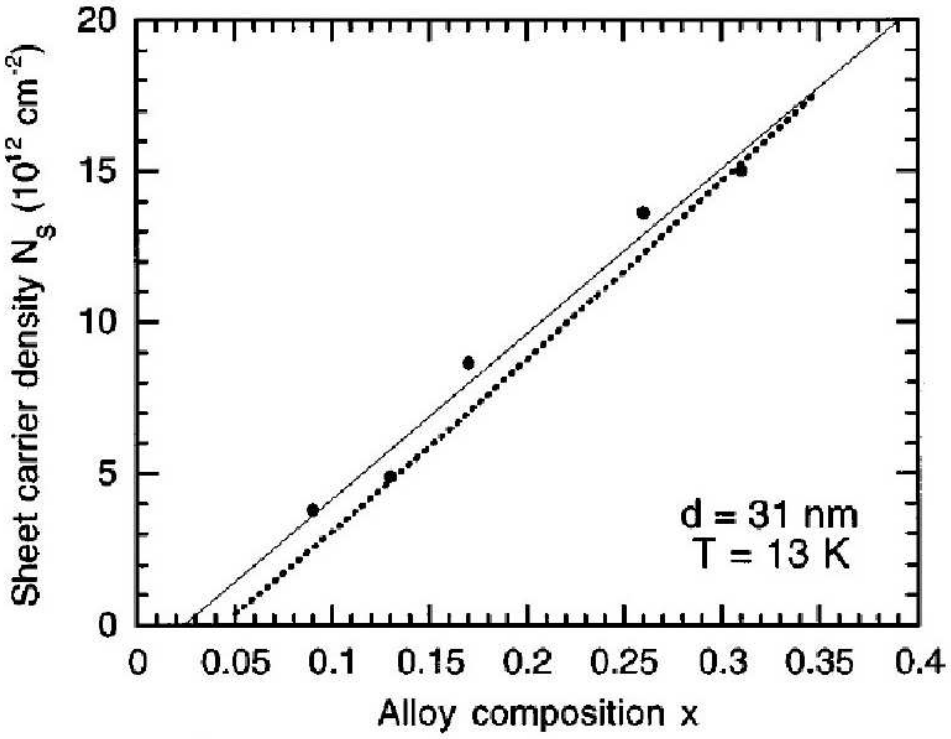

Figure 2.5: 2DEG sheet charge density as a function of AlGaN Al composition [4].

Several researchers have made progress in exploring the mechanism of 2DEG formation. These conjectures indicate that the source of 2DEG includes piezoelectric doping [7], polarization effects coupled with thermal generation [9], unintentional impurities in the AlGaN [11] and donor like traps or states in AlGaN barrier [5]. Though no conclusion about source of 2DEG has been made, properties of AlGaN barrier layer has significant influence on 2DEG density. Figure 2.4 shows measurement of 2DEG as a function of AlGaN barrier thickness from an AlGaN/GaN diode structure with Schottky contact on AlGaN and Ti Ohmic contact on GaN [4]. Measurement of 2DEG density is obtained by C-V measurement. From Figure 2.4 it can be observed that 2DEG forms only when AlGaN barrier thickness is above certain threshold which is about 3nm. Figure 2.5 indicates 2DEG density as a function of Al composition in linear scale under 13K. Despite that physics of formation of 2DEG is not fully understood, it can be observed that 2DEG is strongly controlled by AlGaN barrier thickness and Al composition.

2.4 Mechanism of GaN HEMT

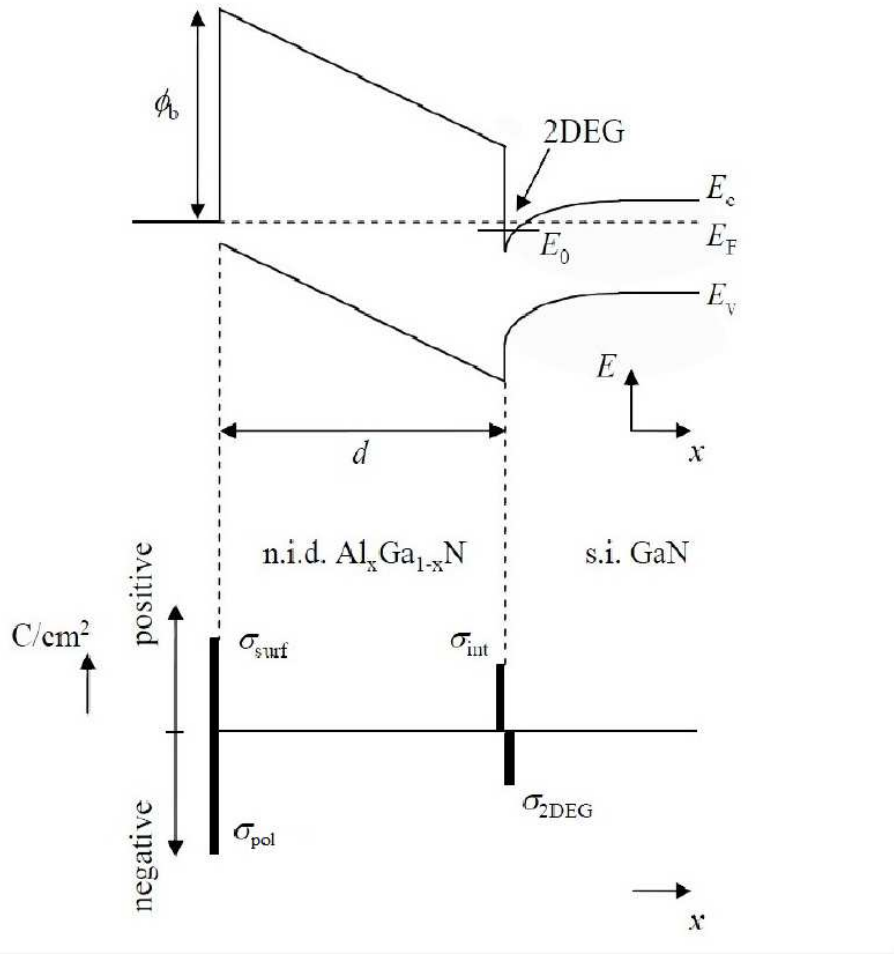

Figure 2.6: Band diagram of heterojunction interface and charge distribution [1].

Figure 2.6 shows the band diagram of AlGaN/GaN heterojunction interface. In Figure 2.6, negative charge σ_{pol} in the upper layer of AlGaN is the sum of piezoelectric and spontaneous polarization charge. The positive charge σ_{surf} represents the donor like surface state which will compensate negative polarization charge of AlGaN. Positive charge σ_{int} represents the net polarization charge at the AlGaN/GaN heterointerface. Since polarization charge is positive in AlGaN lower layer and is larger in magnitude than negative polarization charge in GaN, the sign of σ_{int} is positive. In Figure 2.6, at AlGaN/GaN interface, conduction band is below Fermi level of AlGaN which indicates accumulation of large amount of electrons

at interface. Negative charge σ_{2DEG} represents the two dimensional electron gas which is induced by the excess positive charge in AlGaN/GaN heterointerface. This high density of electron with high electron mobility plays the role of conducting current.

Density of 2DEG can be controlled by applying voltage to gate contact which is located at the top of the structure. While no voltage applied, Fermi level E_f lies at 0 voltage as shown in Figure 2.6. If the gate contact is negatively biased, E_f will go down to negative value which will decrease electron density. As higher negative bias applied to gate contact, eventually E_f will be below conduction band energy level E_c which will result in depletion of 2DEG. The negative voltage which leads to device pinch-off is called threshold voltage V_T.

2.5 Traps in GaN HEMT

Researches show that traps in GaN are one of the essential factors that cause the current degradation in GaN HEMTs. Studies indicate that trapping and de-trapping effect are responsible for the increment of formation of quasi-static charge distribution that makes the current-voltage characteristics at microwave frequencies lower than under direct current condition [12]. In this section, a detail discussion in trap definition, types of traps, spatial and energy locations of traps and their effects in GaN I-V characteristics will be demonstrated.

Figure 2.7 and Figure 2.8 show various traps in crystal structure [1]. One of the origin of traps is the limitation of hetero epitaxy growth technology. Traps in the bulk could be result of dislocation, missing rows of atoms, atom vacancy, self interstitial and impurity interstitial. At heterointerface, traps are generated with high possibility due to lattice constrain occurring between different layers. Other possible trap locations inside the AlGaN/GaN layer are first reported by Khan et al [12], [1] including:

- the semi-insulating substrate(in the case of growth on SiC)
- at the interface between GaN and the substrate (either sapphire or SiC)
- in the non-intentional-doped high-resistivity GaN buffer (deep traps result from good insulation)

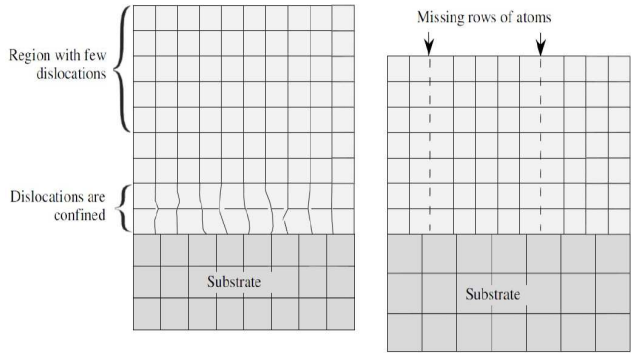

Figure 2.7: Traps in crystal, Left: traps caused by dislocation, Right: traps caused by missing row of atoms [1].

- at the AlGaN/GaN interface
- in the AlGaN barrier layer (bulk trap)

Although sources of traps, trap properties and their effects are not fully understood, controlling of traps is essential to the performance of devices. The following subsections will demonstrate the main kinds of traps in HEMT and degradation involved by those traps.

2.5.1 GaN bulk traps

Bulk traps are also called deep level traps. Typically, GaN buffer region has a background electron concentration due to the presence of oxygen and nitrogen vacancies [13]. Source of oxygen is impurities presence in NH_3 and metal-organic precursors used in MOCVD growth and residual water vapor in MBE or MOCVD chamber [14]. Those presence of electrons in bulk GaN region provide path for current flowing in substrate and furthermore cause buffer or substrate leakage which will result in degradation in pinch-off characteristics.

In order to achieve good insulation in bulk region, Fermi-level of GaN in bulk region is required to be located at the intrinsic Fermi-level of GaN. Although GaN of high purity has Fermi-level that is just located at the intrinsic Fermi-level, it is impossible to obtain extremely

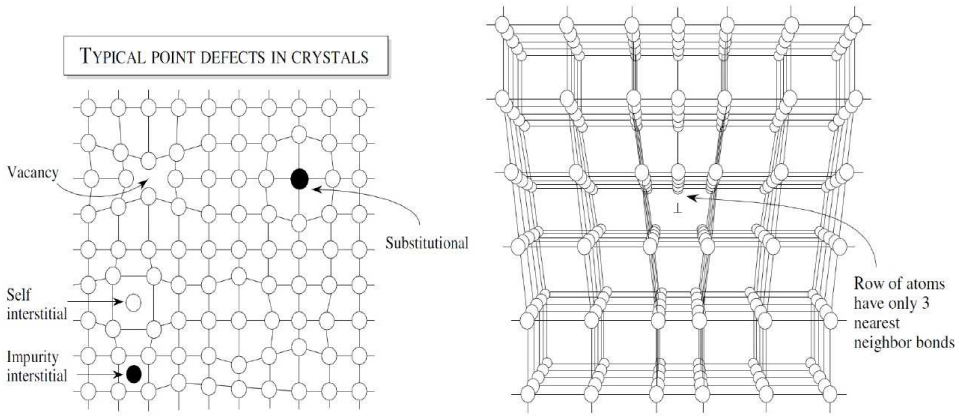

Figure 2.8: Left: point defect traps, Right: volumetric dislocation.

pure GaN in real fabrication process. The idea here is to minimize electron concentration of bulk region, which in another way is to pin the Fermi-level of bulk GaN close to the intrinsic Fermi-level. That is the main reason to introduce acceptor impurity into GaN bulk to compensate with residual electron, and furthermore maintain good insulation. From fabrication point of view, compensation process will be introduced by adding acceptor-like impurities which is the dominant source of deep traps in GaN bulk region. The accurate properties of deep traps are still unclear. Various papers on photo ionization report that GaN buffer layer that grown for GaN MESFET and HEMT have deep traps are 1.8 eV and 2.8 eV below the conduction band as the two main trap centers [15], [16], [17], [18].

2.5.2 AlGaN barrier traps

Recent studies do not indicate much detail and progress in AlGaN barrier traps. Researches report the existence of AlGaN barrier trap with an activation energy of 0.57 eV from the conduction band and is responsible for the performance degradations in [1] and [18]. Those traps provide path between gate and channel that will further deplete channel current carriers which finally leads to degradation of drain current.

2.5.3 Surface traps

Another influential trap in AlGaN/GaN HEMT is the surface trap or surface donor like state which is considered to be the main contributing cause of degradations including gate-lag and DC to RF dispersion. Although evidence of existence of surface trap in AlGaN/GaN HEMT is demonstrated in various papers; the exact type, accurate energy level and mechanism remain unclear [19].

Cause of surface traps on the top layer of AlGaN is the strong strain between GaN cap layer and AlGaN barrier layer. Also, under high voltage beneath gate region traps are generated since large stress is induced by high field [23], [24]. Moreover, crystallographic defects are formed when elastic energy exceeds critical value, large amount of defects will be generated at the heterojunction interface due to lattice mismatch. Those traps are responsible for performance degradation.

Surface traps can be classified into two sorts: intrinsic traps and defects related states [1]. The term intrinsic means that these states will exist even on an ideally perfect surface without defects. They correspond to solutions of Schrodinger's equations with energy levels within the forbidden gap or imaginary values of the wave vector k: the wave functions are evanescent waves that decay exponentially with distance and exist only at the surface. Extrinsic trap, on the contrary is related to the surface defects and impurities occur during crystal growth. The type of surface trap is reported to be donor type in [20], [21] and [22].

2.6 Effects of traps

2.6.1 Current collapse

Current collapse in AlGaN/GaN HEMTs is first discovered by comparison of DC current voltage characteristics before and after high drain voltage is applied. Degradation in current is reported after high drain to source voltage stress is applied. Device is kept under high

drain to source voltage for instance 20 V and zero gate bias for long time. Current recovery could be observed while illuminated by the light with wavelength around 600 nm [14].

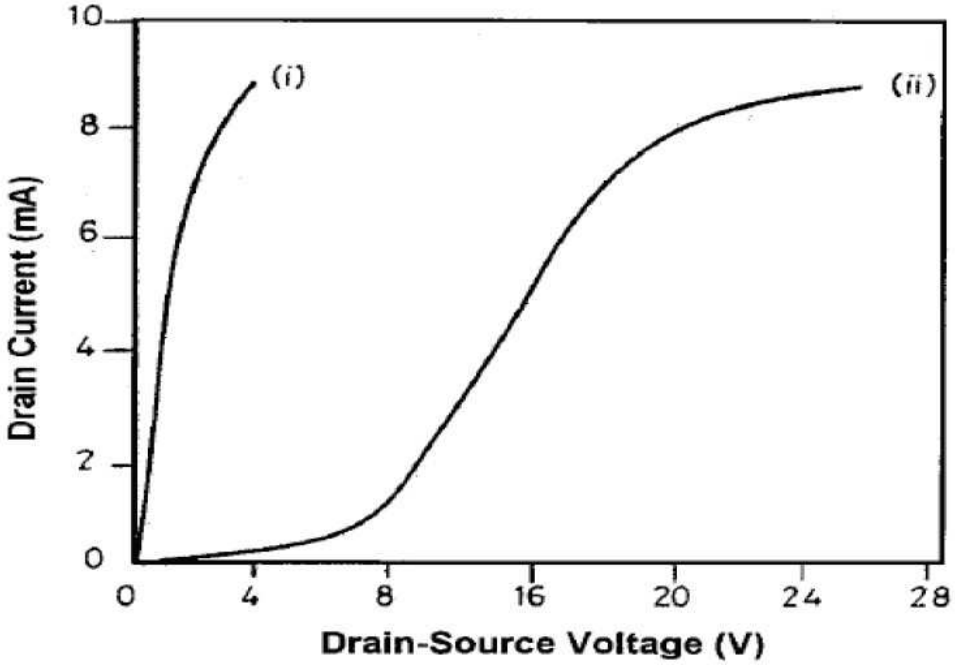

Figure 2.9: Current collapse in GaN HEMTs. $I_d - V_d$ before (i) and after (ii) a drain bias of 20 V is applied [26].

Figure 2.9 shows the current collapse effect due to the deep bulk traps in GaN obtained by measuring HEMT DC characteristics before and after voltage stress of 20V being applied to drain contact. As discussed in the previous subsection of bulk traps, if the conclusion about bulk traps is true, device will present a resistive characteristic due to high trap concentration. In Figure 2.9, after applying voltage stress to HEMT, strong resistive property is observed from curve (ii) which proves the existence of deep bulk traps in GaN. Figure 2.10 and Figure 2.11 show the DC characteristics of voltage stressed HEMT before and after exposing to light illumination. From figure 2.10 and 2.11, evidence show that deep bulk traps are responsible for the current collapse under high drain voltage stress.

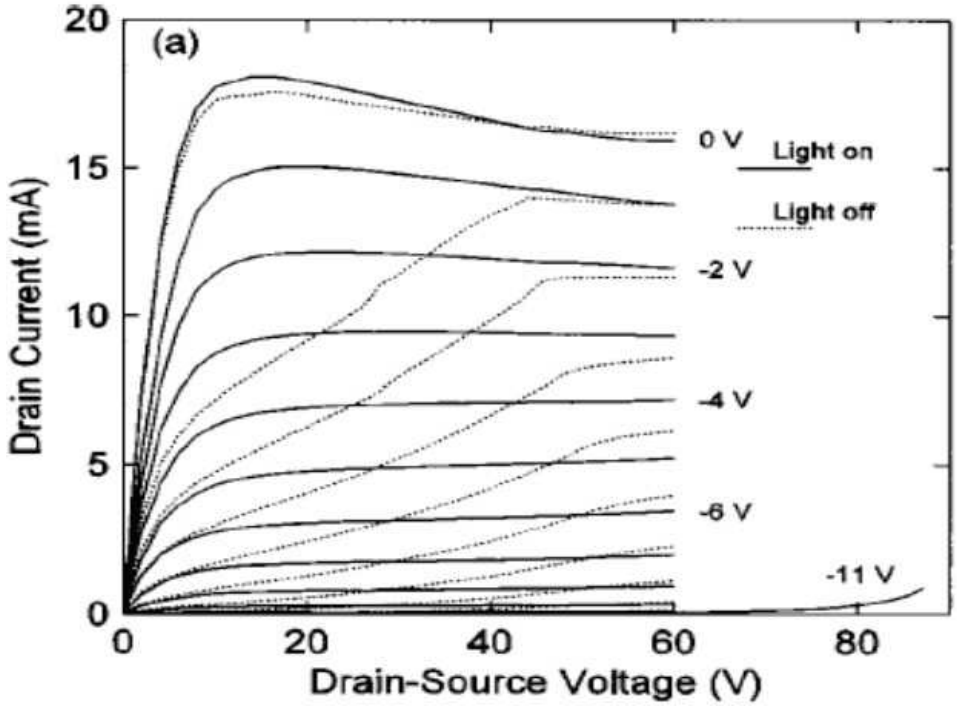

Figure 2.10: Current collapse in GaN HEMTs, with (solid) and without (dash) light illumination [20].

2.6.2 Gate-lag

Gate-lag is defined as the reduction in the drain current observed in the pulsed $I_d - V_d$ characteristics relative to DC measurements made at the same bias point[14].Pulsed-gate $I_d - V_d$ measurements are made by keeping the drain voltage constant and pulsing the gate from the off to on state. Several papers report the surface traps are responsible for gate-lag and gate-lag can be reduced by annealing and inclusion of passivation layer. Figure 2.12 and 2.13 show the pulsed $I_d - V_d$ measurement of HEMTs with and without passivation layer respectively. Device with passivation layer performs better in pulsed $I_d - V_d$ measurement which provides evidence for the improvement trap density by Nitride passivation layer [22].

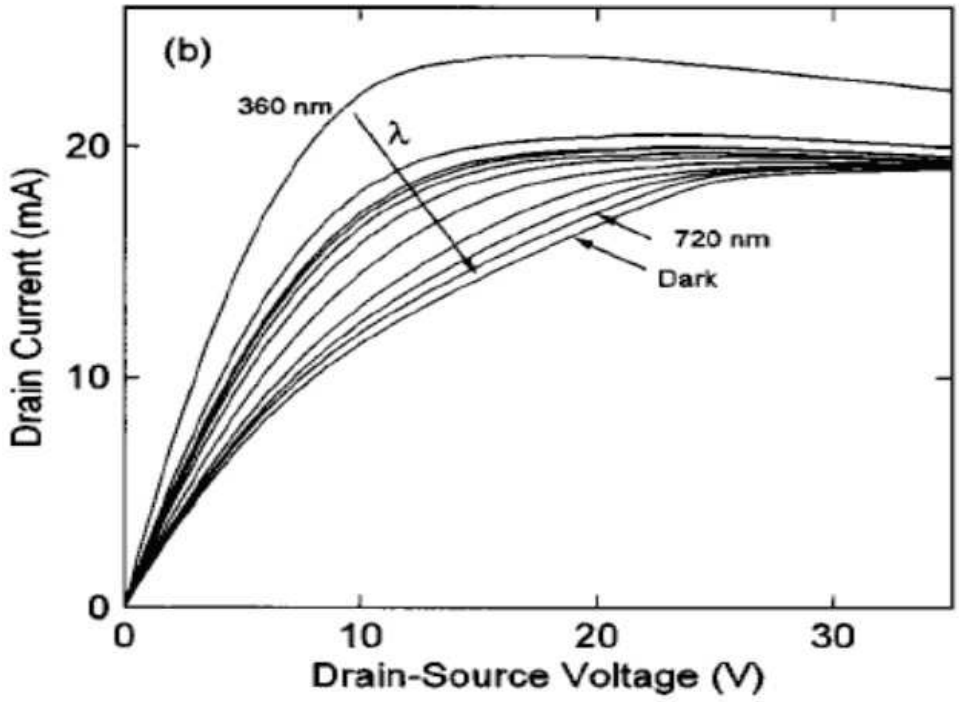

Figure 2.11: Current recovery dependence of wavelength of light illumination.

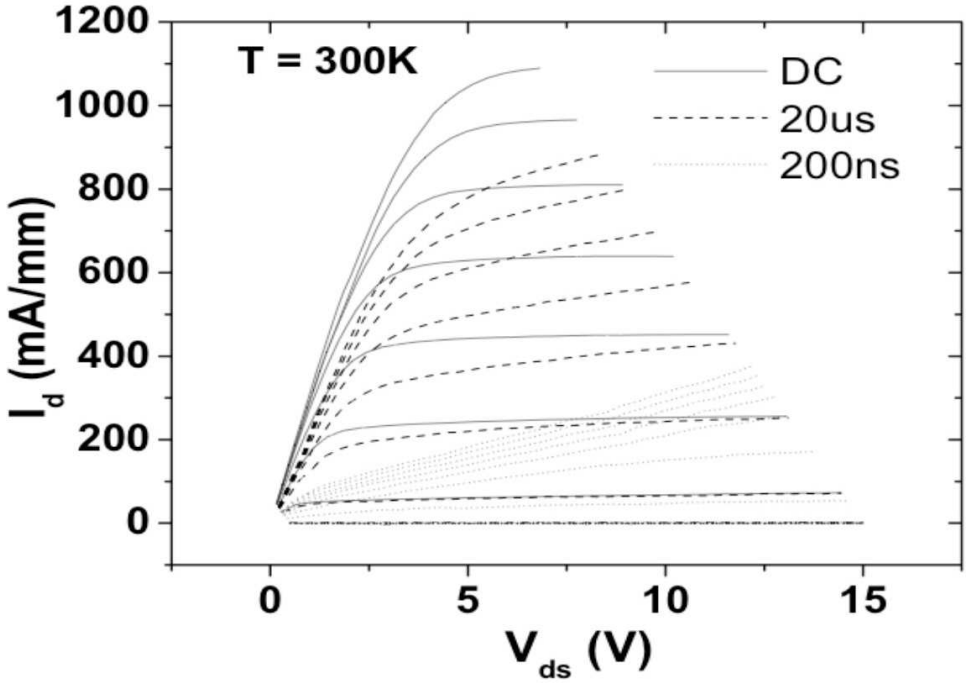

Figure 2.12: Pulsed $I_d - V_d$ characteristics for an unpassivated GaN HEMT [25].

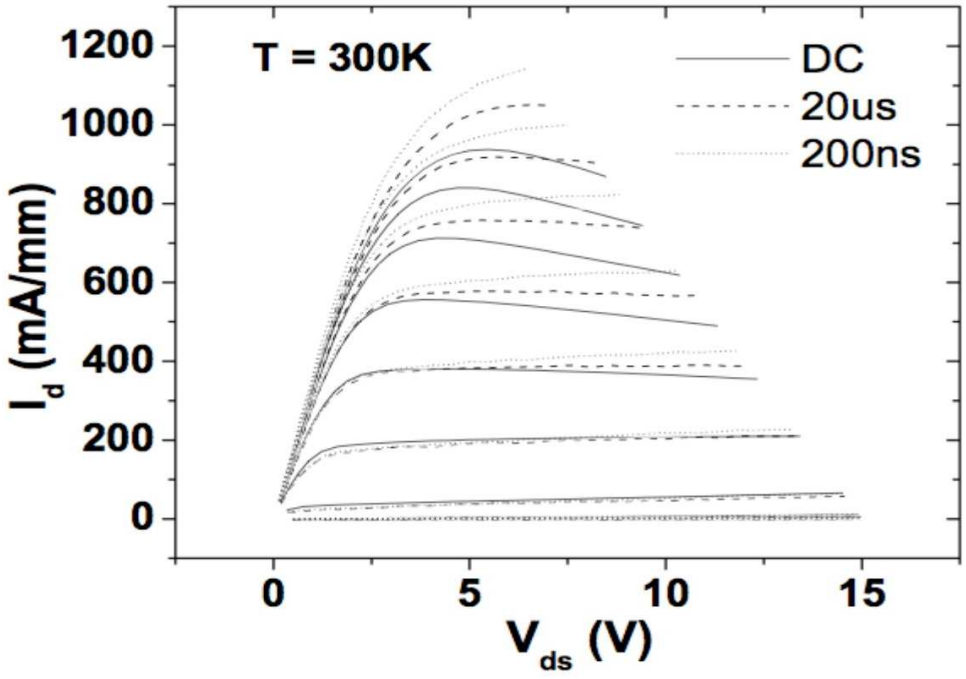

Figure 2.13: Pulsed $I_d - V_d$ characteristics of a passivated GaN HEMT [25].

Chapter 3

AlGaN/GaN HEMT simulation

Simulation is performed in Sentaurus version 2012.09 [27]. Svisual is used to visualize simulation results. The first step is to create a 2D HEMTs structure with proper mesh in Sentaurus Structure Editor. Physics models are applied to the structure in Sdevice. Generally the simulation result should consist of DC output simulation which is often known as $I_d - V_d$ and $I_d - V_g$, AC simulation for high frequency characteristics and transient simulation of which trap is a key influential factor. Only DC simulation will be presented in this work. Later, attempts to achieve gate length scaling are examined in this work in DC output simulation. There are two approach for polarization charge placement in simulation. One approach is to use built-in model provided by simulator, the other approach is to add TCL code calculating polarization charge density for each material and place charge manually in each layer. Manual charge placement approach is used for matching measurements since real device is cylindrical and built-in model does not support cylindrical coordinate simulation with anisotropic axis.

3.1 Device Structure

The HEMTs in this work are all cylindrical. Figure 3.1 is a photograph of HEMTs in various sizes. The dark brown small circle located at center of each device is drain contact, the outer circle is the source contact, bright yellow part is metal contact of gate.

Table 3.1 shows the geometries of fabricated cylindrical HEMT. In Table 3.1, L_{gd} refers to the distance between gate and drain, and L_{sg} refers to the distance between source and gate. L_g refers to the length of gate.

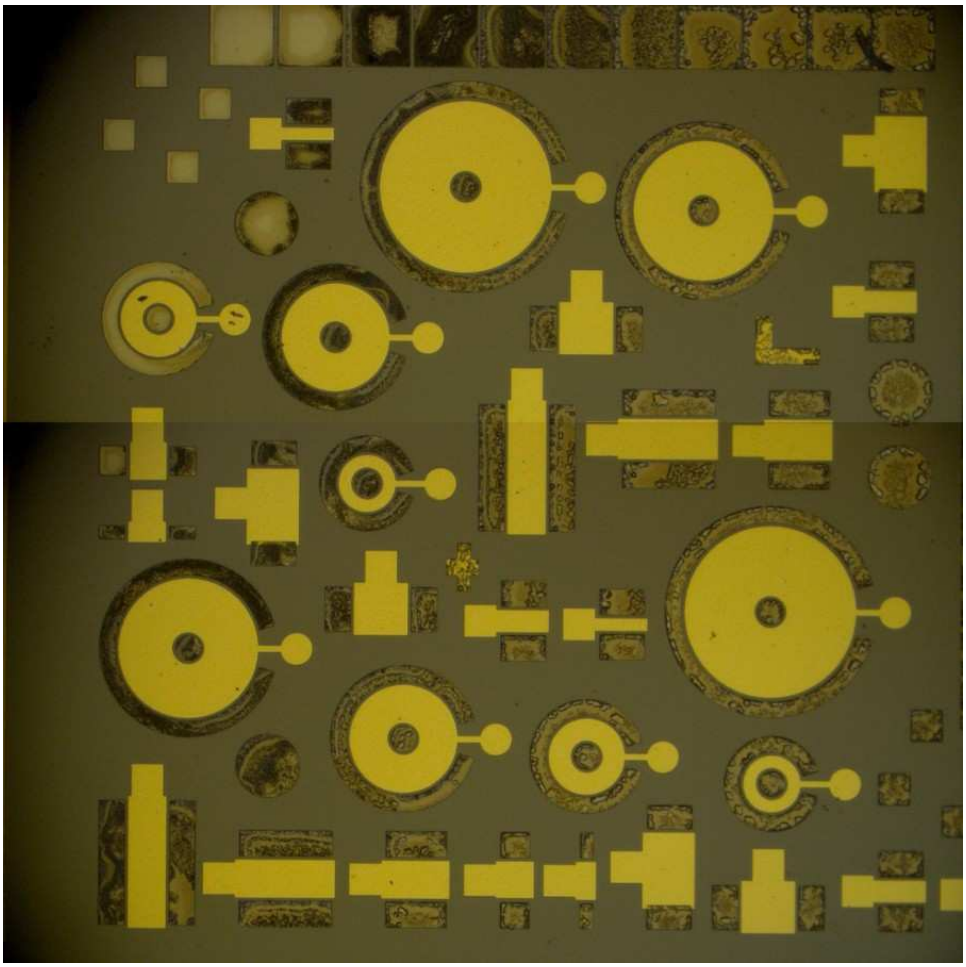

Figure 3.1: HEMT device die photo.

Device Number	L_{gd} (um)	L_{sg} (um)	L_g (um)
1 and 6	10	10	220
2 and 7	10	10	170
3 and 8	10	10	120
4 and 9	10	10	70
5 and 10	10	10	40

Table 3.1: Dimension of HEMT.

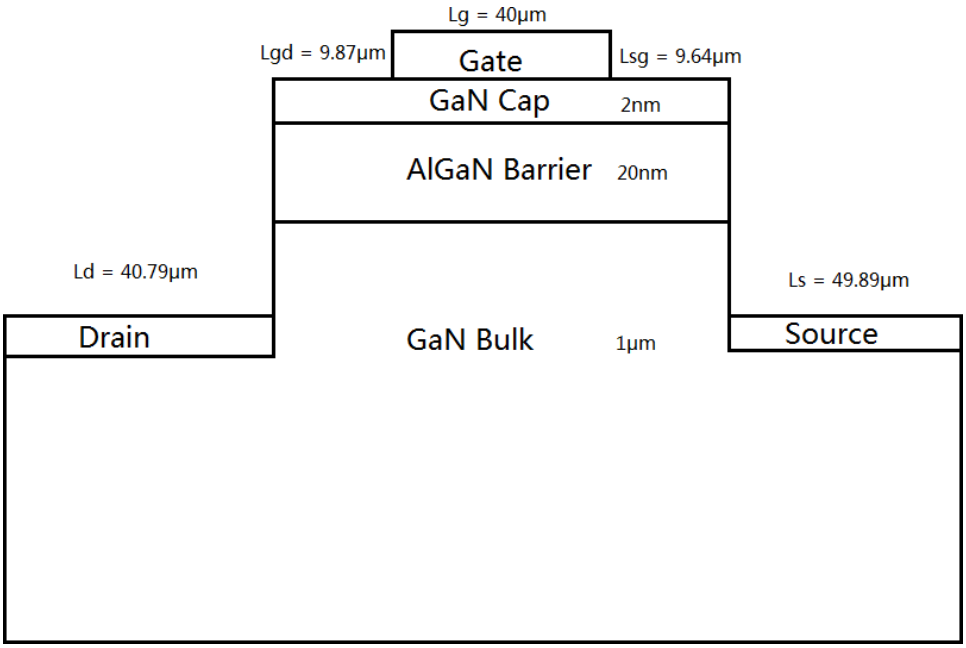

Figure 3.2: Schematic diagram of AlGaN/GaN HEMT studied in this work.

Figure 3.2 shows the schematic diagram of the HEMT studied. The substrate of the structure is specified as oxide,buffer layer is GaN which has a lower mobility compared with channel region GaN. The top of GaN buffer layer is channel which directly connects to AlGaN barrier layer. The heterojunction interface between GaN channel and AlGaN barrier is essential part of the device which requires refined mesh which will be illustrated in the Meshing subsection in order to properly simulate the characteristics of the device. A 2 nm GaN cap layer is placed on the top of AlGaN barrier. Some commercial GaN HEMTs contain an additional layer that called passivation layer that consists of nitride. It is reported that lower trap density can be achieved by growing passivation layer on top of GaN cap layer. To simplify the process of adding trap to GaN cap layer, Ni passivation layer is constructed in simulation.

To match measurements, some adjustments are introduced during the simulation. Adjustments include electron mobility of channel GaN, barrier height of gate metal, dopant type and doping concentration in GaN. Furthermore, in obtaining polarization charge density and 2DEG density, two different approaches of charge placement are presented in this work.

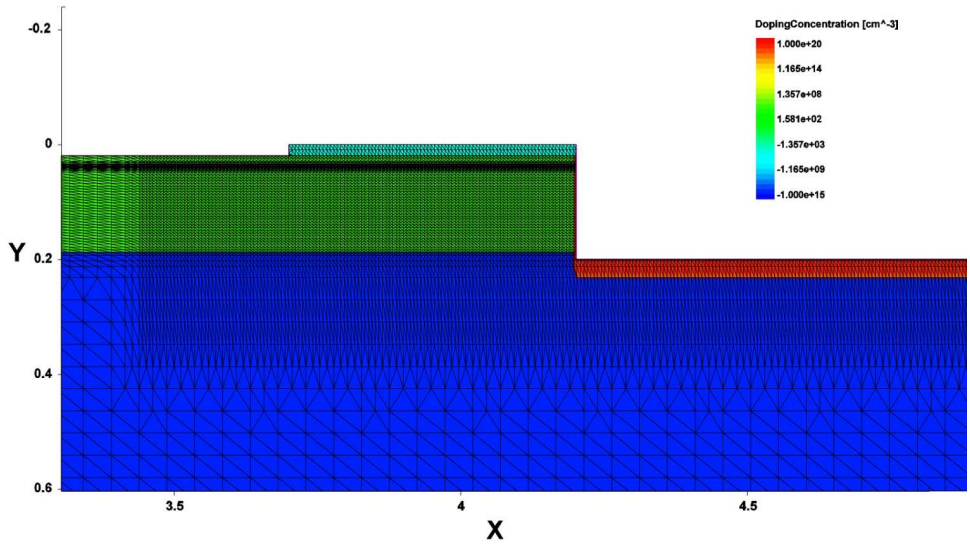

Figure 3.3: Refined mesh at heterojunction interface.

Sentaurus simulator itself contains an adjustable built-in model of polarization charge calculation consisting of spontaneous polarization charge and piezoelectric polarization charge. The second approach of obtaining polarization charge is through Sentaurus Workbench by adding TCL script that calculates polarization at the beginning of sdevice command file, then placing each portion of calculated polarization charge density to respective region in the device. The calculation of polarization charge is based on Equation (2.3), Equation (2.4) and Equation (2.5).

3.2 Device structure building

3.2.1 Meshing

Meshing needs to be extreme intense at the interface of GaN buffer and AlGaN barrier where the 2DEG locates. At the gate contact edge deep below the channel region, meshing is also required to be refined. In those regions, changes of parameters such as electron density, electric field and current density are huge. To simulate the properties of those regions, mesh need to be intense enough. Figure 3.3 illustrates a refined mesh at the heterojunction interface and contacts. In Figure 3.3, thin layers of intense mesh are presented at the

AlGaN/GaN heterojunction interface and gate contact edge. Besides those regions, mesh is not so dense for the goal of reducing calculation in simulation. Good mesh should on one hand be dense in the region where fast changes of parameters occur, on the other hand, be minimum to reduce simulation time. For example, the mesh of HEMT structure in this thesis is homogeneous intense at beginning. The amount of elements in mesh is roughly 100,000. It consumes over 1 hour for simulating a complete $I_d - V_g$ curve when V_d is ramped to 5 V and V_g is swept from -5 V to 5 V. Then, meshing in regions where parameters change slowly is gradually reduced. Time consumption is expected to decrease with less elements in mesh. The final refined mesh of HEMT contains nearly 20,000 elements. Simulation will fail due to convergence issue with mesh that contains elements less than the final refined mesh. The error in Poisson equation and carrier density can be observed using error print. The largest error locates at the interface of passivation layer and GaN cap where mesh is reduced. Time consumption for final refined mesh to finish the same $I_d - V_g$ simulation is roughly 25 min.

3.2.2 Charge calculation and placement

Spontaneous polarization effect exists in the whole region of both AlGaN and GaN. It is mole fraction dependent and varies with the composition of each element in the material. Piezoelectric polarization effect is generated from the heterojunction interface lattice mismatch between two layers. Two approaches of charge calculations and placements are presented in this subsection. The first approach is applying built-in polarization model in the simulator. Parameters in polarization charge equation such as piezoelectric coefficients are modified in a separate parameter file. Once built-in model is activated, simulator will automatically calculate charge densities in each layer and place them respectively. The charge equation used to calculate polarization charge is marked as Formula 2 in simulator which is defined in separate parameter file as well. The second approach is to use the same charge equation to calculate sum polarization charge density at each interface and place charge as fixed trap into corresponding interface. Parameters used in manual charge placement in

charge calculation are set to be identical to the built-in model. TCL command that used for charge calculation is shown below:

```
# Calculation of polarization charge
set q = 1.602e-19 ;
set x = @x@;
set strainRelax = @relax@;

# Mole fraction dependent spontaneous polarization
set Psp_AlN =  -8.1E-6/q;
set Psp_GaN = -2.9E-6/q;
set Psp_AlGaN = x*Psp_AlN + (1 - x)*Psp_GaN ;
set DPsp = Psp_GaN - Psp_AlGaN;

# Mole fraction dependent piezo electric polarization
#AlN
# e31 = -5.0e-5
# e33 = 1.79e-4
# c13 = 1.08e11 = 108 GPa
# c33 = 3.73e11 = 373 GPa

# GaN
# e31 = -3.5e-5
# e33 = 1.27e-4
# c13 = 1.06e11 = 106 GPa
# c33 = 3.98e11 = 398 GPa

set e31i =(x * (-0.50E-4) + (1 - x) * (-0.35E-4))/ q ;
```

```
set e33i = (x * 1.79E-4 + (1 - x) * 1.27E-4) / q ;
set c13i = x * 108 + (1 - x) * 106 ;
set c33i = x * 373 + (1 - x) * 398 ;

set straini = (1- strainRelax) * (x * (3.189 - 3.112) / (x * 3.112 + (1- x) * 3.189 )
set Ppz_AlGaN = 2* straini * ( e31i - c13i / c33i * e33i ) ;

set DPpz = -Ppz_AlGaN ;
set intCharge = DPsp + DPpz ;

set AlGaN_Spontaneous = Psp_AlGaN
set AlGaN_Piezoelectirc = Ppz_AlGaN

set GaN_Spontaneous = Psp_GaN

set Total_AlGaN = Psp_AlGaN + Ppz_AlGaN

set AlGaN_GaN_Interface = intCharge

set AlGaN_Nitride_Interface = Total_AlGaN
```

One important thing should be noticed if using built-in model for simulation. Polarization charge at bottom layer of GaN almost has no influence on 2DEG density since thickness of bulk GaN is 1 micron which is relatively large compared with the heterojunction structure which is less than 100 nm. In other words, particularly in this structure, there is no polarization charge at the bottom layer of GaN. In Sentaurus device, if the key word piezoelectric

written in the scripts, the simulator will automatically turn on all the piezoelectric polarization effect at all region interface even there should not be any polarization effect between certain interfaces. To solve this problem, one line of command is inserted to the script to eliminate the incorrect interface simulation:

```
Physics (MaterialInterface = "GaN/Oxide")
{Piezoelectric polarization (activation = 0)}
```

For both built-in model and manual charge placement, lattice axis, simulation axis and anisotropic direction need to be defined. Lattice axis is defined in separate parameter file, simulation axis and anisotropic direction are modified in Sdevice command file. The command used to modify those parameters is shown as below:

```
# Define lattice parameters for all materials outside of any material or region
LatticeParameters {
X = (1, 0, 0)
Y = (0, 0,-1)
}

# Also define Piezoelectric polarization Formula=2 outside of any material
# it is used for all regions in the simulation
Piezoelectric_Polarization {
Formula= 2
}


# Define anisotropic epsilon for GaN and AlN
Material= "GaN" {
```

```
Epsilon
{ * Ratio of the permittivities of material and vacuum
  * epsilon() = epsilon
epsilon = 9.5 # [1]
}

Epsilon_Aniso
{ * Ratio of the permittivities of material and vacuum
  * epsilon() = epsilon
epsilon = 10.4 # [1]
}
}



Material= "AlN" {
Epsilon
{ * Ratio of the permittivities of material and vacuum
  * epsilon() = epsilon
epsilon = 9.0 # [1]
}

Epsilon_Aniso
{ * Ratio of the permittivities of material and vacuum
  * epsilon() = epsilon
epsilon = 10.7 # [1]
}
```

$P_{sp}[C/cm^2]$ in AlGaN	-0.042
$P_{sp}[C/cm^2]$ in GaN	-0.029

Table 3.2: Spontaneous polarization in AlGaN and GaN.

C11 $[GPa]$	391.5
C12 $[GPa]$	143.0
C13 $[GPa]$	106.5
C33 $[GPa]$	391.6
e31 $[C/cm^2]$	$-3.189 \cdot 10^{-5}$
e33 $[C/cm^2]$	$1.4 \cdot 10^{-4}$

Table 3.3: Piezoelectric polarization coefficients and stiffness constants in AlGaN.

```
}
```

```
Aniso (Poisson direction (0, 0, 1))
```

Table 3.5 shows the spontaneous polarization of AlGaN and GaN that are used in built-in model and manual charge density calculation. Table 3.6 shows piezoelectric polarization coefficients and stiffness constants in AlGaN barrier that used during simulation. Modifying parameters in built-in model is achieved by editing a separate parameter file. In built-in model, polarization model can be active by using the commands shown below. Relaxation factor is modified from default value 0.1 to 0 in the separate parameter file to achieve the maximum piezoelectric polarization charge due to stain.

```
    Piezoelectric_Polarization (strain)
```

```
# Modified in separate parameter file inside material parameter modification
```

a_0	3.189
a	3.16975
$Relax$	0.0

Table 3.4: Strain parameters and relaxation parameter.

```
Material= "GaN" {
Piezoelectric_Polarization
relax = 0.0
}

Material= "AlN" {
Piezoelectric_Polarization
relax = 0.0
}
```

To validate manual charge placement, dummy structures including single layer of AlGaN, AlGaN/GaN heterojunction layer and GaN/AlGaN/GaN triple layer structure are constructed to explore the relation between polarization charge density obtained using built-in model and manual charge placement. Currentplot section in TCAD can be used to attract additional data in a specified region. To detect the polarization charge in each layer, the following command is included in sdevice file. In the command shown below,

```
PE_polarization
```

total polarization in a specified material consisting of spontaneous polarization and piezopolarization. The word *Integrate* will enable simulator to output the integral of polarization charge over the specify the region. In the command shown below, integration window is specified at the middle of the x dimension in each layer.

```
CurrentPlot {
 PE_polarization(
Integrate(Name = "PE_GaN_cap" Window[(0.4 0.49 0) (0.6 0.5 0)]) )
    }
```

Dividing the integral by the integration range in x dimension, polarization charge in sheet charge density format can be obtained. The default integration unit is um which will

give the integral an unit of um^2 / cm^3 which is $10^{-8}/cm$. By changing the integration unit to cm, the final result will have the unit of $/cm$. The command used to change integration unit is modified in Math section shown as below:

```
Math {
    CurrentPlot (IntegrationUnit = cm )
}
```

To manually place charge at interface, commands shown below are applied:

```
Physics {
    (MaterialInterface = "AlGaN/GaN")
    {Traps ( FixedCharge Conc = !(puts Conc )! )  }
   }
```

The sheet charge of concentration $Conc$ is obtained from the manual calculation based on Al mole fraction. Assumption that there is no relaxation between AlGaN and GaN interface has been made during calculation. In other words, it is the maximum polarization charge that can exist at the heterojunction interface.

Equations used for polarization charge calculation are shown as below:

$$\sigma = P(AlGaN) - P(GaN) = P_{SP}(AlGaN) + P_{PE}(AlGaN) - P_{SP}(GaN)C/cm^2 \quad (3.1)$$

$$P_{PE} = 2\frac{a - a_0}{a_0}(e_{31} - e_{33}\frac{C_{13}}{C_{33}})C/cm^2 \quad (3.2)$$

Mole fraction of Al (x)	P_{sp} ($C/\ cm^2$)	P_{pz} ($C/\ cm^2$)	Sum ($C/\ cm^2$)
0	-2.9· 10^{-6}	0· 10^{-6}	-2.9· 10^{-6}
0.2	-3.9· 10^{-6}	-0.73· 10^{-6}	-4.67· 10^{-6}
0.4	-4.98· 10^{-6}	-1.593· 10^{-6}	-6.57· 10^{-6}
0.6	-6.02· 10^{-6}	-2.592· 10^{-6}	-8.62· 10^{-6}
0.8	-7.06· 10^{-6}	-3.742· 10^{-6}	-10.8· 10^{-6}
1.0	-8.1· 10^{-6}	-5.039· 10^{-6}	-13.14· 10^{-6}

Table 3.5: Piezoelectric polarization and spontaneous polarization in AlGaN.

Mole fraction of Al (x)	P_{sp} charge density ($/cm^2$)	P_{pz} charge density ($/cm^2$)	Sum ($/cm^2$)
0	-1.8102· 10^{13}	0· 10^{13}	-1.8102· 10^{13}
0.2	-2.4594· 10^{13}	-0.4556· 10^{13}	-2.9150· 10^{13}
0.4	-3.1086· 10^{13}	-0.9945· 10^{13}	-4.1031· 10^{13}
0.6	-3.7578· 10^{13}	-1.6201· 10^{13}	-5.3779· 10^{13}
0.8	-4.4070· 10^{13}	-2.3359· 10^{13}	-6.7429· 10^{13}
1.0	-5.0562· 10^{13}	-3.1455· 10^{13}	-8.2017· 10^{13}

Table 3.6: Piezoelectric polarization and spontaneous polarization charge densities in AlGaN.

$$P_{SP}(x) = -0.052x - 0.029C/cm^2 \tag{3.3}$$

$$P_{SP}(0) = -0.029C/cm^2 \tag{3.4}$$

$$\sigma(x) = 2\frac{a - a_0}{a_0}(e_{31} - e_{33}\frac{C_{13}}{C_{33}}) + P_{SP}(x) + P_{SP}(0) \tag{3.5}$$

Based on Al mole fraction, spontaneous polarization, piezoelectric polarization, spontaneous polarization charge density and piezoelectric polarization charge density are calculated and shown in Table 3.5 and Table 3.6.

Compared with the corresponding results from built-in model, a perfect match can be achieved. The simulation results of built-in model polarization of Al mole fraction of 0.4 are shown in Figure 3.4.

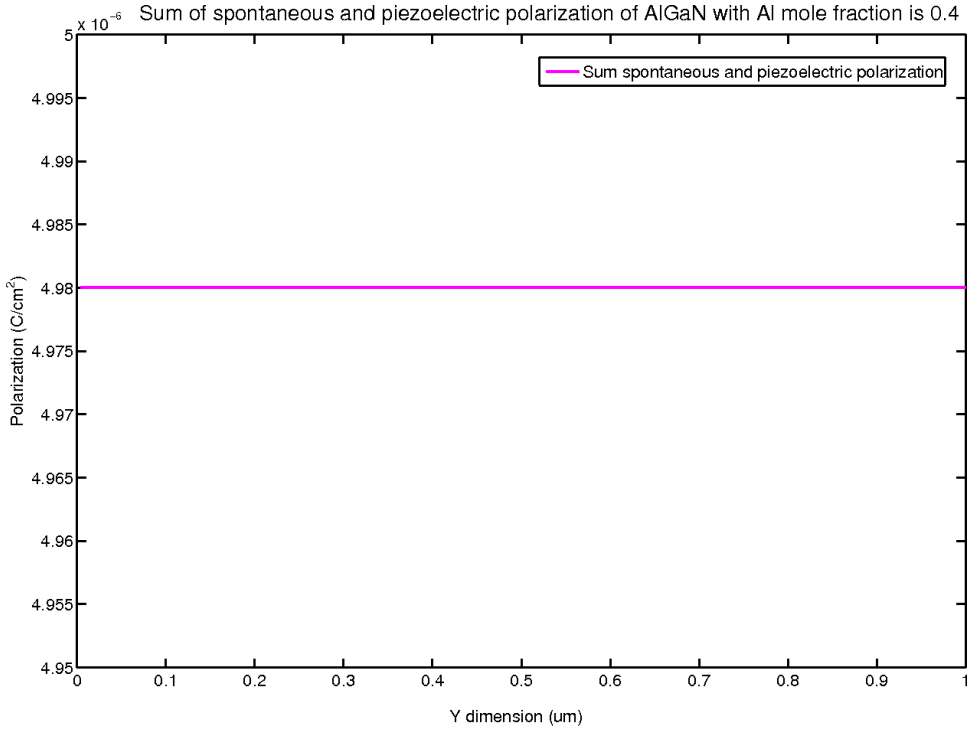

Figure 3.4: Sum of spontaneous and piezoelectric polarization in AlGaN with Al mole fraction is 0.4.

Figure 3.4 shows the polarization in AlGaN. In AlGaN, spontaneous polarization is pointing from upper edge to lower edge which causes the spontaneous polarization induced charge being negative in upper edge while being positive at the lower edge. Since in single layer of AlGaN, the whole region has the same lattice constant. There is no strain or stress effect in the material which leads to the zero piezoelectric polarization in the material. From Figure 3.4, it can be observed that the sum of polarization is equal to spontaneous polarization in single layer structure. The sum of polarization is -4.98 C/cm^2 which is identical to the value obtained from manual charge placement in Table 3.5.

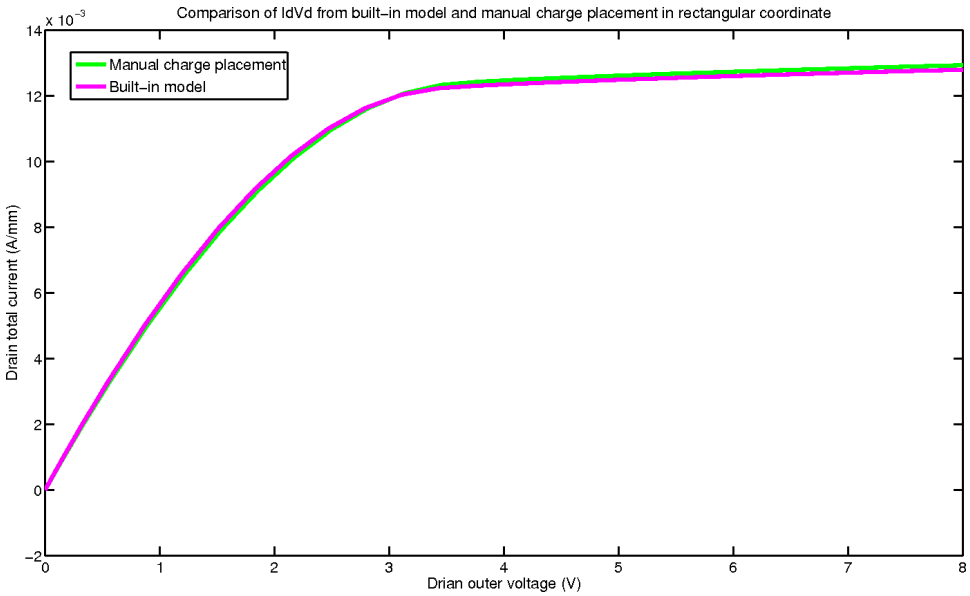

Figure 3.5: Comparison of $I_d - V_d$ simulation results from manual charge placement and built in model in rectangular coordinate.

Simulation results using built-in model and manual charge placement in rectangular coordinate are compared in Figure 3.5. In Figure 3.5, the magenta curve presents the simulation result from built-in model and the green curve is the corresponding result for using manual charge placement method. From Figure 3.5 it can be observed that simulation results from built-in model matches with that from manual charge placement. This observation proves manual charge placement method producing correct polarization charge density.

In this subsection, a comparison between manual charge calculation and built-in model charge is presented. In triple layer of GaN/AlGaN/GaN, polarization charge density obtained from the built-in model in each layer is identical to the charge density calculated using piezoelectric polarization charge equation. This conclusion justifies using manual charge placement instead of built-in model in further simulation when built-in model fails in cylindrical coordinate.

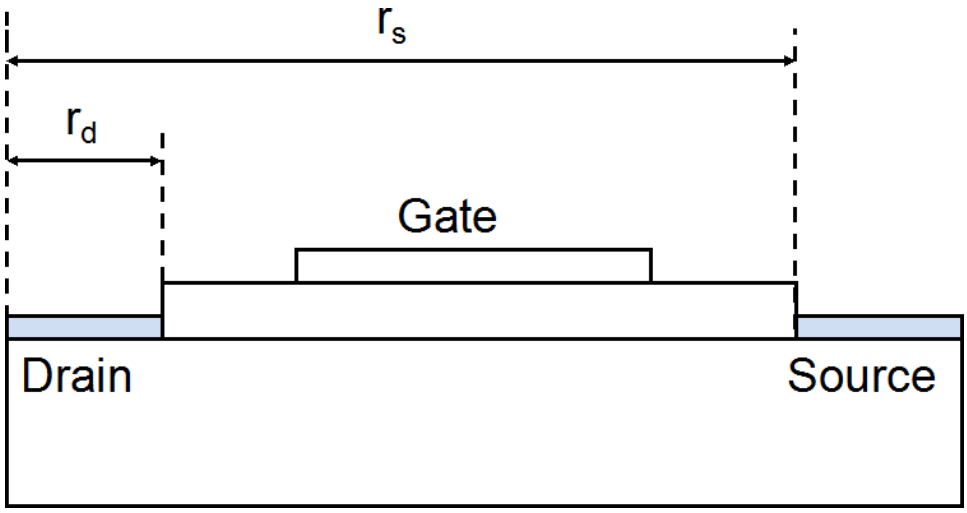

Figure 3.6: Cross-sectional view of cylindrical HEMT along vertical direction (half structure).

3.2.3 Conversion from cylindrical coordinate to rectangular coordinate

The cross-sectional view of cylindrical HEMT (half structure) is shown in Figure 3.6. In Figure 3.6, r_d is the distance from center of cylindrical HEMT to the edge of drain contact which is also the radius of circular drain contact. r_s is the distance from center of cylindrical HEMT to inner edge of source contact.

Equation (3.6) and Equation (3.7) show simplified equations for rectangular MOSFET channel current calculation. A HEMT is similar in Equation (3.6) and Equation (3.7), I_{DS} is the current in the channel of a rectangular MOSFET or HEMT. μ is the electron mobility in the channel, W is the channel width, L is the channel length and C_{ox} is capacitance per unit area of channel. V_{GS} represents the gate to source voltage, V_T is the threshold voltage to turn on the device and V_{DS} is drain voltage.

$$I_{DS} = \frac{W}{L} \cdot \mu \cdot C_{ox} \cdot (V_{GS} - V_T - \frac{1}{2}V_{DS}) \cdot V_{DS} \quad \text{if } V_{DS} \leq (V_{GS} \text{ - } V_T) \tag{3.6}$$

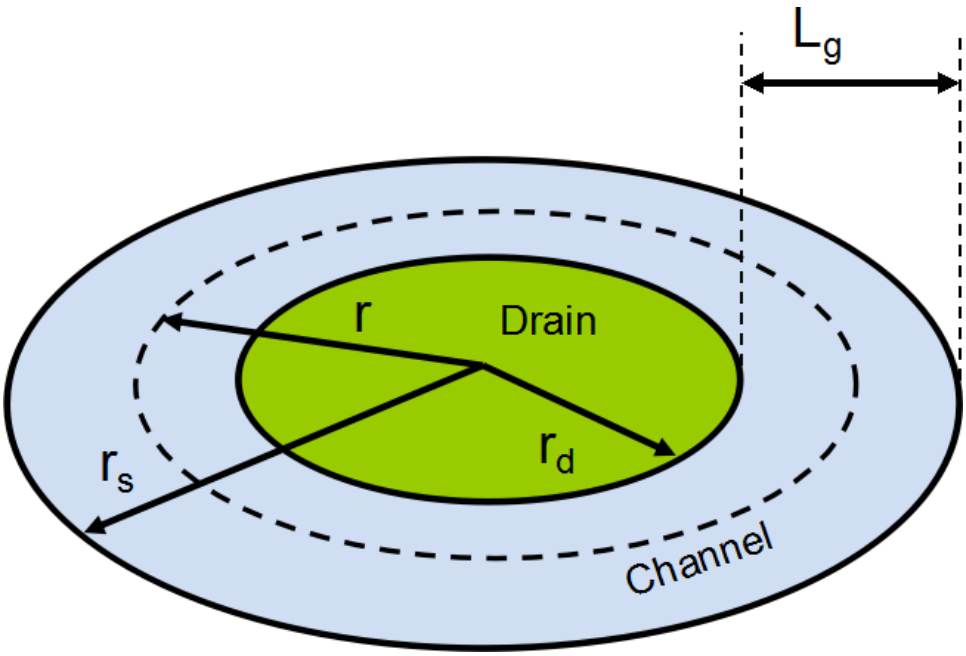

Figure 3.7: Top view of drain and channel region of cylindrical HEMT.

$$I_{DS} = \frac{W}{L} \cdot \mu \cdot C_{ox} \cdot \frac{1}{2}(V_{GS} - V_T)^2 \quad \text{if } V_{DS} \geq (V_{GS} \text{ - } V_T) \tag{3.7}$$

To make the form of current calculation in cylindrical coordinate similar to the rectangular current calculation, some assumptions and simplifications can be made. Firstly, the capacitance per unit area of the channel is a constant. HEMT can be divided into infinite numbers of ring like structures with different radii r as shown in Figure 3.7. Considering the symmetry in cylindrical structure, current will flow from center of circular drain to the circular source. The cross-sectional view cut along direction of current flowing of cylindrical HEMT is shown in Figure 3.6 that is similar to a cross-section of rectangular HEMT. The equation for cylindrical coordinate current calculation is shown in Equation.(3.8) and Equation (3.9). In Equation.(3.8) and Equation (3.9), $I_{DScylin}$ is the channel current in cylindrical coordinate.

$$I_{DScylin} = \cdot\mu \cdot C_{ox} \cdot (V_{GS} - V_T - \frac{1}{2}V_{DS}) \cdot V_{DS} \cdot \int \frac{2\pi r}{dr} \quad \text{if } V_{DS} \leq (V_{GS} \text{ - } V_T) \tag{3.8}$$

$$I_{DScylin} = \cdot\mu \cdot C_{ox} \cdot \frac{1}{2}(V_{GS} - V_T)^2 \cdot \int \frac{2\pi r}{dr} \quad \text{if } V_{DS} \geq (V_{GS} \text{ - } V_T) \tag{3.9}$$

Moving the integration related to r to the left side of equation, a relation between r and channel length and width can be achieved. The simplified relation is shown in Equation (3.10) and Equation (3.11). In Equation (3.10) and Equation (3.11), r_s represents the distance from the origin (symmetry axis) to the channel outer edge, while r_d represents the distance from symmetry axis to channel inner edge.

$$\frac{L}{W} = \frac{1}{2\pi} \int_{r_s}^{r_d} \frac{dr}{r} \tag{3.10}$$

$$\frac{L}{W} = \frac{1}{2\pi} \ln \frac{r_s}{r_d} \tag{3.11}$$

$$W_{eff} = \frac{W}{L} \cdot L_g = 2 \cdot \pi \cdot \frac{L_g}{\ln \frac{r_s}{r_d}} \tag{3.12}$$

For the device that needs to be simulated, r_d equals to 40 um, r_s is 100 um while gate length L_g is 40 um. Plugging in r_s and r_d values into Equation.3.12, W_{eff} equals to 427.35 which is the effective channel width. In simulation, channel width can be defined as area factor in the Physics section for rectangular HFET simulation. By default, area factor

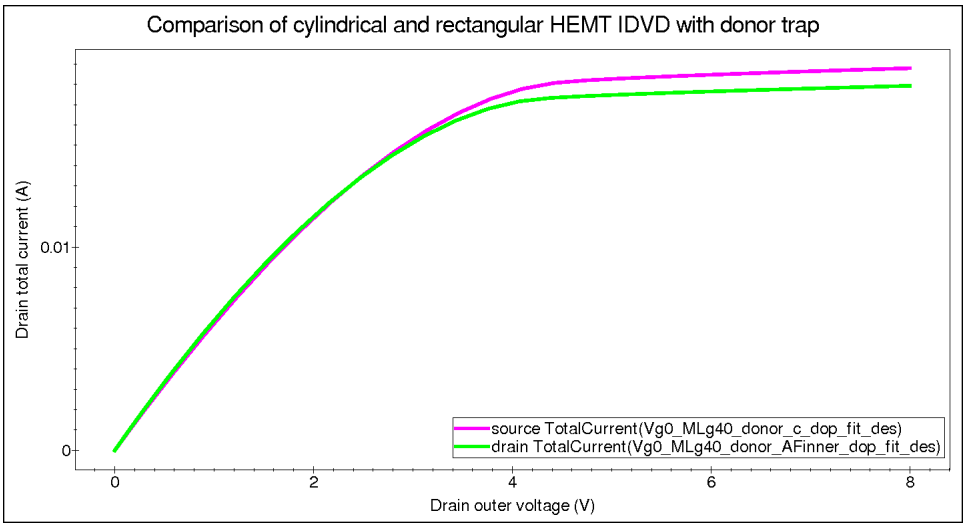

Figure 3.8: Comparison of cylindrical and rectangular HEMT $I_d - V_d$ with donor trap and n-type doped buffer.

is 1 um in simulation if no specification is made in command file. To make comparison between the effective rectangular HFET simulation model with cylindrical model, area factor in rectangular model simulation is modified to be the value of W_{eff}. Simulation result of comparison of manual charge placement HEMT in cylindrical and rectangular coordinate is shown in Figure 3.8.

In Figure 3.8, the magenta curve represents the $I_d - V_d$ simulation result for cylindrical coordinate while the green curve is the corresponding result for rectangular coordinate. From Figure 3.8, it can be observed that two curve fit each other well in the linear region but have some variation in saturation region. When drain voltage is relative low, electrons in channel are distributed as a function that only relates to location. In another words, electron distribution is only a function respected to r which is the distance from certain point to the symmetry axis. Thus the approximation in Equation (3.12) is valid. When drain voltage is increasing until saturation region, charge distribution in channel is influenced by drain voltage. As a result, certain phenomena begin to occur such as pinch-off which furthermore leads to the charge distribution change. Thus approximation in Equation (3.12) fails which is the main reason of the difference in $I_d - V_d$ curve in saturation region between cylindrical

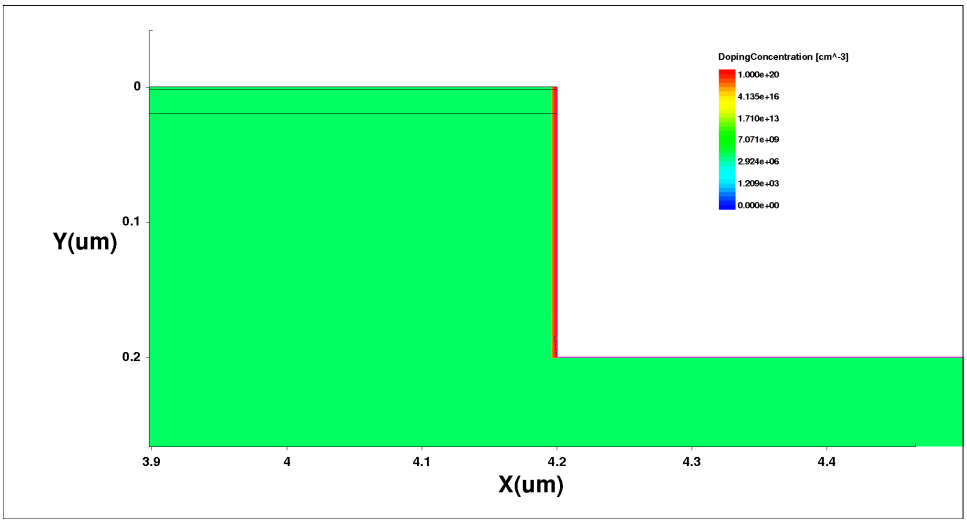

Figure 3.9: HEMT structure with n-type doped buffer.

and rectangular HEMTs. The approximation is less valid under high voltage or for short channel device.

3.2.4 Leakage current

Figure 3.9 shows the HEMT structure with n-type doped buffer which is the starting point of the simulation. The goal of adding n-type dopant is to simulate the effect of impurities in GaN buffer since GaN buffer region is not an intrinsic semiconductor even without intentional doping. During the fabrication, GaN buffer region typically will exhibit some degree of n-type conductivity, presumably due to the unintentional doping of residual impurities such as Si and O [1]. By following structure in De Brida Christian's dissertation [1], n-type dopant of concentration $10^{15}/cm^3$ is applied to GaN buffer region to simulate the residual impurities introduced during fabrication. In addition, to achieve better convergence, highly n-type doped contacts of concentration $10^{20}/cm^3$ are applied to both drain and source sides. Convergence issue will be discussed later in convergence subsection.

Figure 3.10 shows simulation result of $I_d - V_g$ curve of HEMT with n-type doped buffer of which doping concentration is $10^{15}/cm^3$. Figure 3.11 shows the same curve under logarithmic

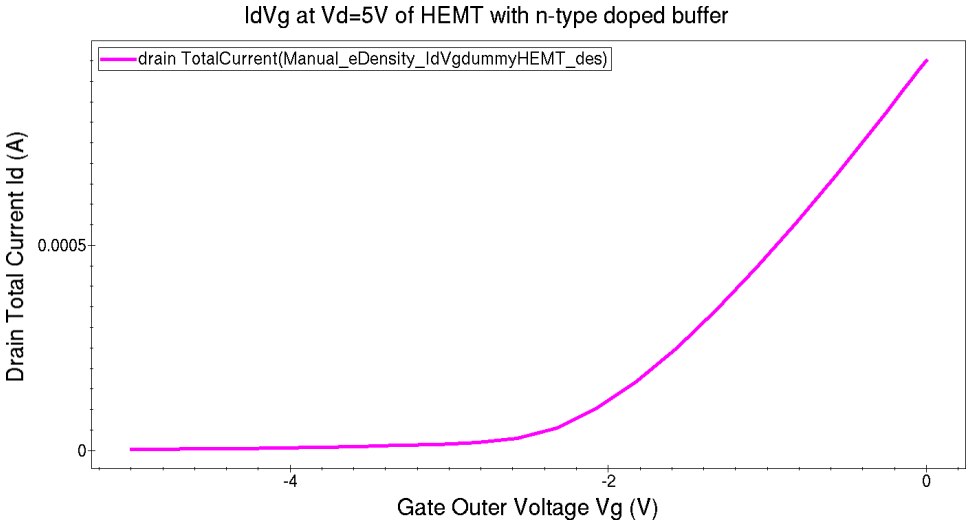

Figure 3.10: $I_d - V_g$ curve of n-type doping buffer in linear scale ($V_d = 5$V).

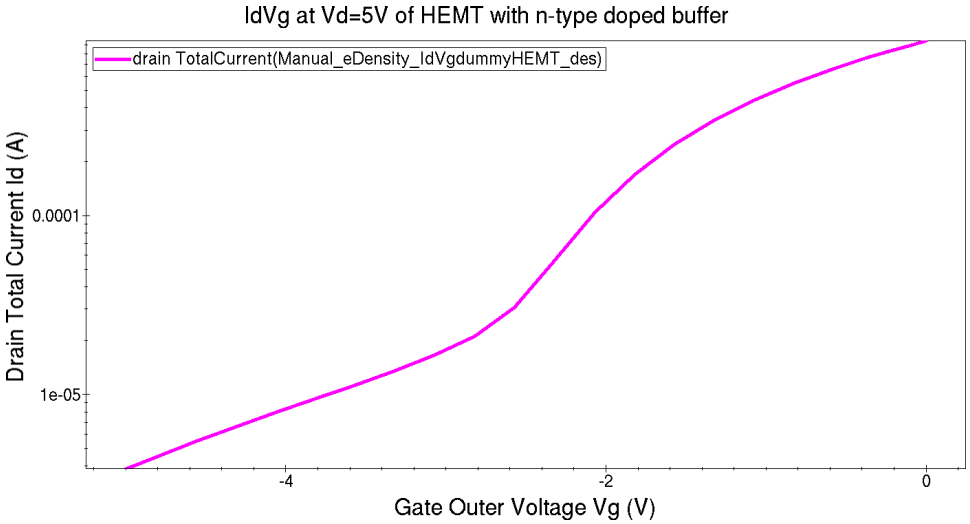

Figure 3.11: $I_d - V_g$ curve of n-type doping buffer in logarithmic scale ($V_d = 5$V).

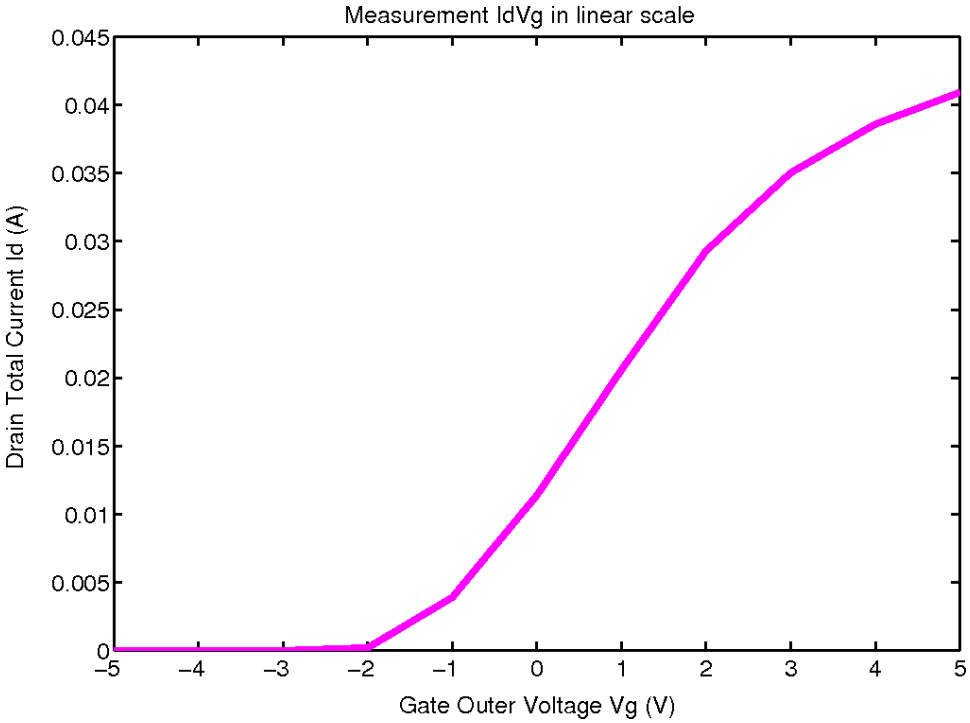

Figure 3.12: $I_d - V_g$ measurement in linear scale ($V_d = 5$V).

scale. There is a noticeable off-state current which indicates that device does not shut-off effectively.

Figure 3.12 and Figure 3.13 show the measurement of $I_d - V_g$ curve in linear scale and logarithmic scale respectively. compared simulation result with measurement, it is clear that off-state current leakage is huge in simulation. Figure 3.14 shows the current density at off-state which is at $V_g = 5$V and $V_d = 5$V. The red color in Figure 3.14 indicates a high current density which distributes among the whole buffer region. Thus, the source of leakage current is n-type dopant in GaN buffer.

In device fabrication, the residual donors in an unintentionally n-doped GaN buffer are compensated by deep acceptor states to obtain high resistivity [1]. To observe influence of buffer dopant on off-state leakage, a parallel simulation with p-type doped buffer is built. Figure 3.15 shows the layer structure of p-type doped buffer, geometry of this structure is identical to the structure in Figure 3.9. Observed from the comparison of simulation results

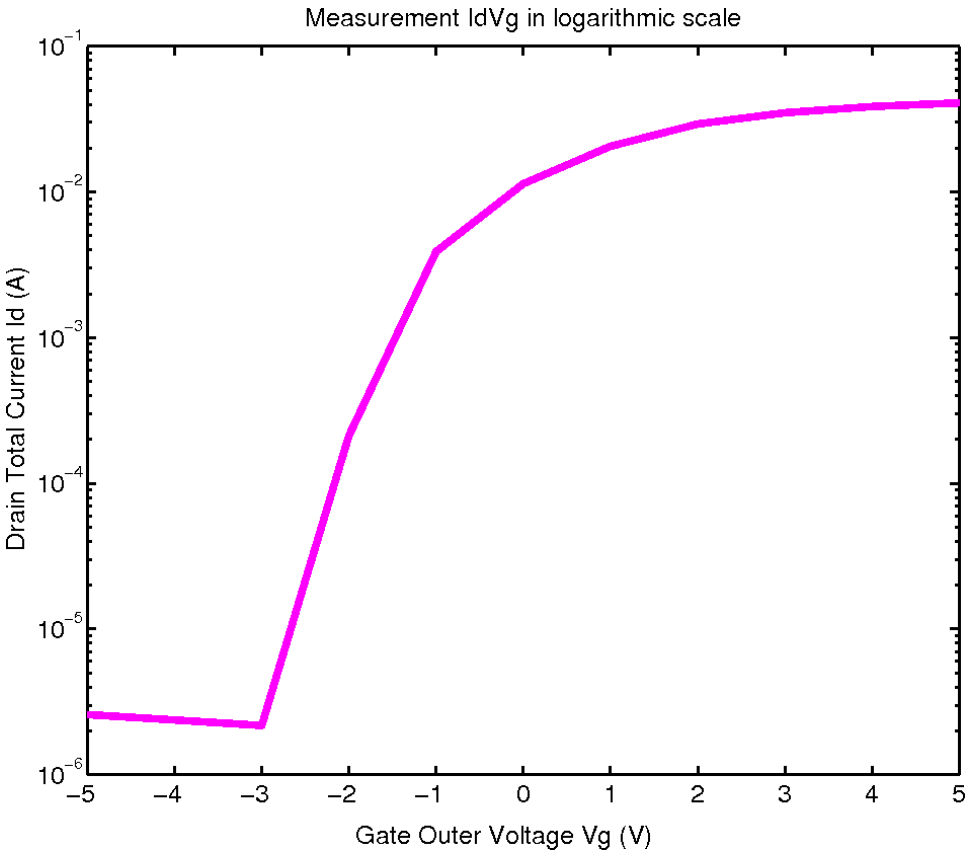

Figure 3.13: $I_d - V_g$ measurement in logarithmic scale ($V_d = 5$V).

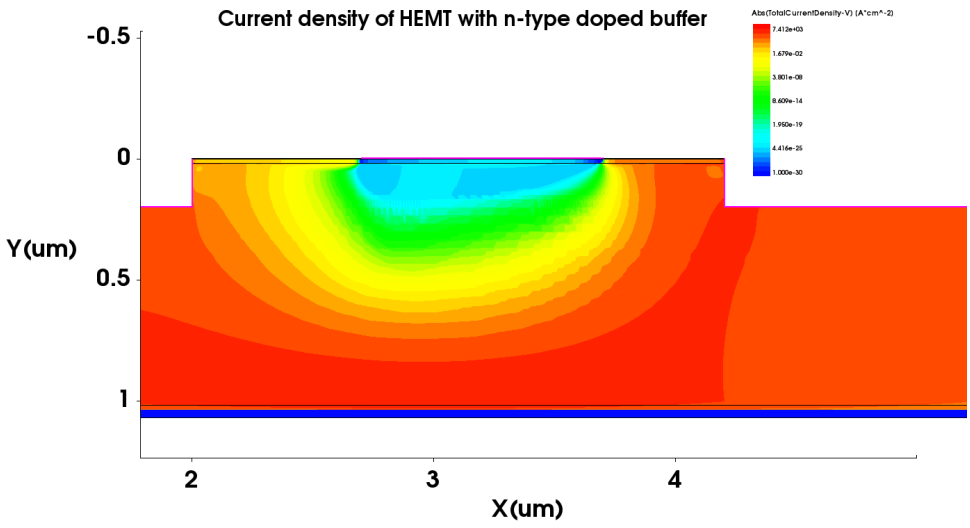

Figure 3.14: Leakage current in buffer region and substrate (n-type doped buffer).

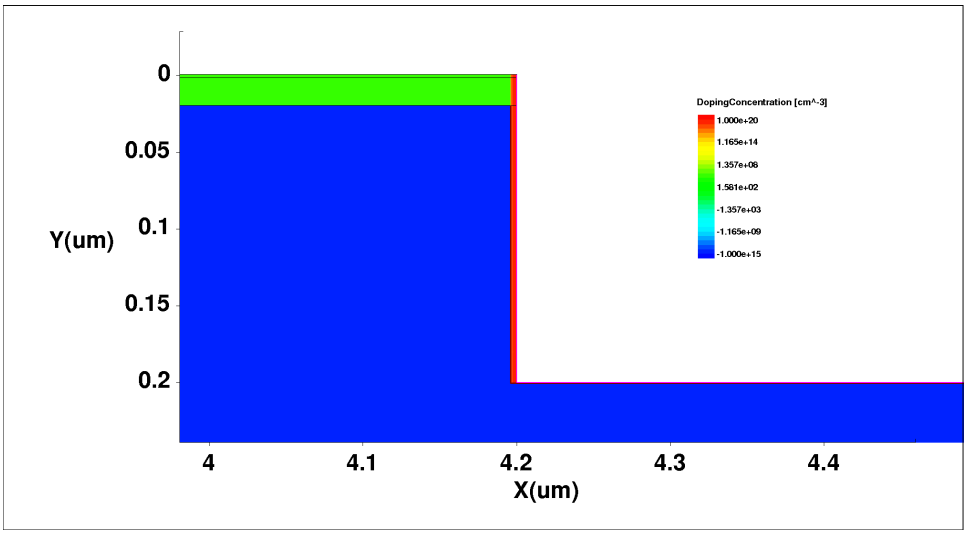

Figure 3.15: Layer structure of HEMT with p-type doped buffer.

from n-type buffer HEMT and p-type buffer HEMT, off-state current leakage is effectively reduced by applying p-type dopant in buffer region.

Figure 3.16 and Figure 3.17 show the comparison of $I_d - V_d$ curves from HEMTs with p-type doped buffer and n-type doped buffer in linear scale and logarithmic scale respectively. In Figure 3.16 and Figure 3.17, blue curve represents the p-type doped device, red curve stands for n-type doped device. Figure 3.18 shows the current density of HEMT with p-typed doped buffer. It can be observed from Figure 3.17, the off-state current of p-type doped device is 10 orders less in magnitude than that of n-type doped device. Although, current density shown in Figure 3.18 indicates current leakage density is reduced by 13 orders in magnitude. Compared simulation result of p-type buffer HEMT with measurement, off-state leakage is significantly small. Conclusion is buffer region of real HEMT device contains no impurities of n-type, instead n-type impurities is contained in channel region. Thus, n-type doping of concentration of 10^{15} $/cm^{-3}$ is applied to GaN channel of simulation HEMT structure.

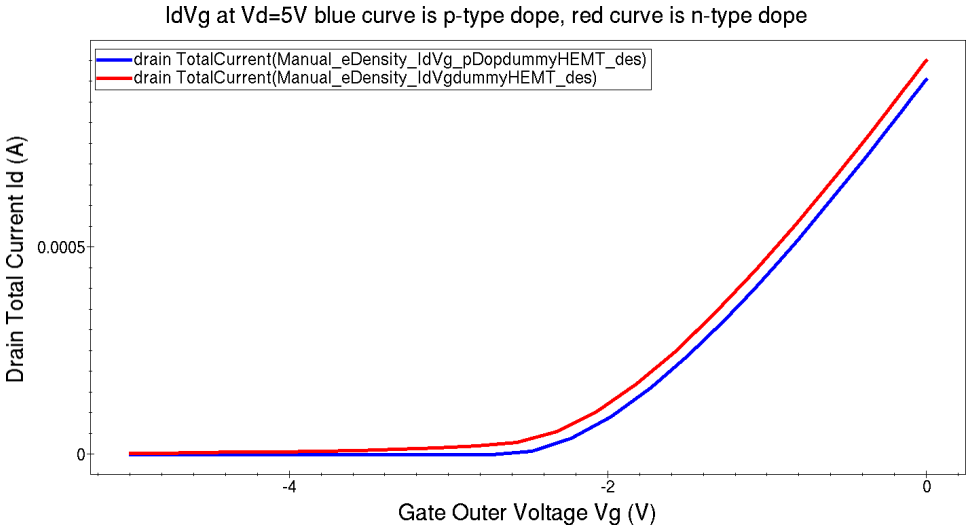

Figure 3.16: $I_d - V_g$ curves of p-type doped buffer and n-type doped buffer HEMT in linear scale ($V_d = 5$V).

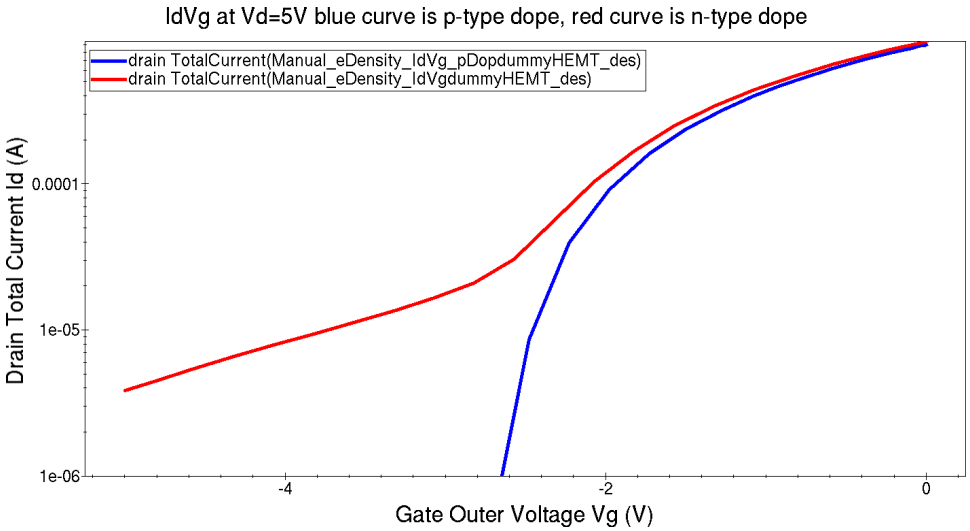

Figure 3.17: $I_d - V_g$ curves of p-type doped buffer and n-type doped buffer HEMT in logarithmic scale ($V_d = 5$V).

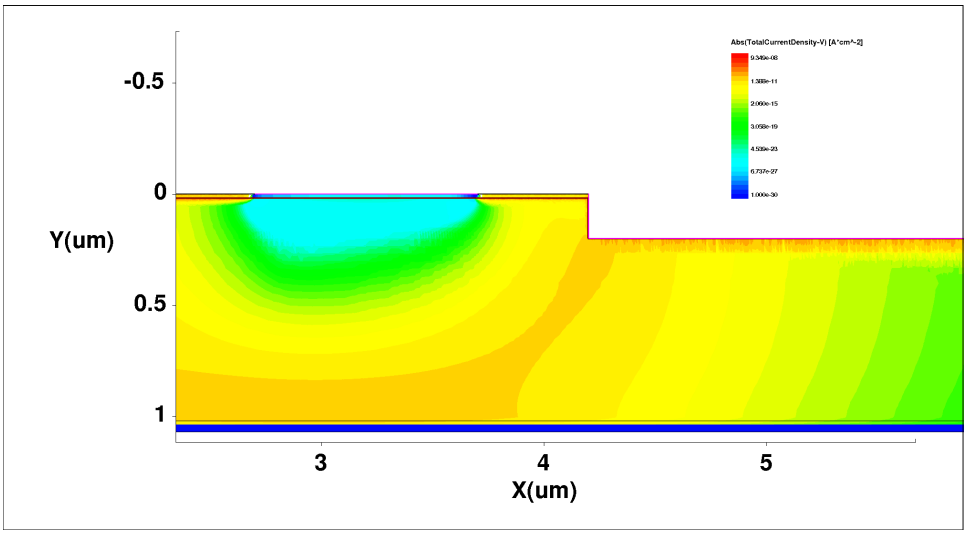

Figure 3.18: Current density of a HEMT with p-type doped buffer.

3.2.5 Convergence control

For wide band-gap material, intrinsic carrier concentration is extremely small compared with conventional semiconductor material such as Si. For this reason convergence issue is one of the obstacles in simulation. Several attempts are introduced during the simulation to solve convergence problem including extended precision digit, tracing maximum update error using CNormPrint, using different meshing grids, applying highly doped semiconductor beneath drain and source contacts and using electron barrier tunneling model for source and drain contacts. Solving convergence problem has been a big issue in this work. The only solution is to build parallel simulation with different combination of extended precision digits, meshing grids, highly n-doped electron barrier tunneling contacts.

From the simulation results, rectangular coordinate system tends to have better convergence than cylindrical one. However, cylindrical coordinate system is still used for simulation. Highly n-type doped contacts with doping concentration equal to $10^{20}/cm^3$ are placed below the metal contacts to achieve better convergence. Electron barrier tunneling model is applied to source and drain contact. Better convergence is achieved by changing source and drain from Ohmic contacts to Schottky contacts with effective masses of AlN and GaN in

contact regions being modified to $0.01m_0$ to reach small resistive contacts. The method is to apply nonlocal mesh to source and drain contacts with tunneling current from electron barrier tunneling current. Effective masses of AlN and GaN are modified to small value only at source and drain contacts in order to modify the tunneling current to reach zero resistive contacts. This modification does not influence the global parameter of effective mass applied in the whole structure other than source and drain contacts. Controlling of source and drain contacts can be achieved by modifying value of effective masses of AlN and GaN in nonlocal mesh region.

Extended precision is modified in Math section. Effective masses in GaN and AlN of nonlocal source and drain are modified in separate parameter file. Schottky drain and source contacts are defined in electrode section. Electron barrier model is activated in Physics section. Command used for modifying extended precision, electron barrier tunneling, Schottky drain source contacts and effective masses are shown in below:

```
    Extrapolate
    Iterations = 20
    ExtendedPrecision
    Digit = 8
    RHS = 1e-10
    CNormPrint
    NewtonPlot(
        Error MinError
        Residual
        )

Electrode {
        { Name="gate"   Voltage= 0 Schottky barrier = 1.5  }
        { Name="source" Voltage= 0 Schottky Workfunction= 4.3 }
        { Name="drain"  Voltage= 0 Schottky Workfunction= 4.3 }
```

```
}


Physics {
eBarrierTunneling "NLM_Source"
eBarrierTunneling "NLM_Drain"
}

Material= "AlN" {
BarrierTunneling {
mt = 0.01, 0.01 # [1]
g = 1,1 # [1]
}
}

Material= "GaN" {
BarrierTunneling {
mt = 0.01, 0.01 # [1]
g = 1,1 # [1]
}
}
```

3.2.6 Trap

Donor trap is inserted to the GaN cap layer during the simulation acting as one of sources of electrons in 2DEG. Except for being one of the sources of electrons in 2DEG, another reason to adding trap during simulation is to reduce resistance series in un-gate

region of the HEMT due to channel shut-off. Donor trap is neutral when occupied by electron, and is carrying positive charge of a hole when empty. When there is no trap in the GaN cap layer, the polarization charges in each layer locate at the edge of each layer. The upper edge of layer is negatively charged and lower edge is positively charged with equal amount of charge as the upper edge. There is no induced charge in each layer in this case.

When donor trap is applied to the GaN cap layer of the device, the negative charge in the upper edge of GaN cap layer is trapped by the donor trap inserted to the layer which will leave excess positive charge at the lower edge of GaN cap. The excess positive charge will compensate with the negative charge in the AlGaN upper edge which will leave excess positive charge at the lower edge of AlGaN. The excess positive charge at lower edge of AlGaN will induce electron at the upper edge of GaN buffer which is the channel of the device. The increment of electron density in the channel will finally lead to the increment of current flowing from source to drain. To prove this scenario, simulations with and without trap are performed. Donor trap of concentration of $5{\cdot}10^{13}\ cm^{-2}$ of various energy levels are applied to the interface of GaN cap and Nitride.

The magenta curve in Figure 3.19 represents the simulation result with donor trap in GaN cap layer while the green curve represents the corresponding result for the simulation without donor trap. It can be observed that the simulation result with donor trap is significantly larger than that without donor trap which is consistent with the scenario.

The comparison of $I_d - V_d$ simulation results with various trap energy is shown in Figure 3.20. In Figure 3.20, the magenta curve represents the $I_d - V_d$ simulation result with trap of energy level locating at 0.4 eV above the middle of energy band. The green curve in Figure 3.20 represents the corresponding simulation result with trap energy level locating at 0.4 eV below the middle of energy band. In the simulation matching measurement subsection, trap density and trap energy level are adjusted to fit the measurement.

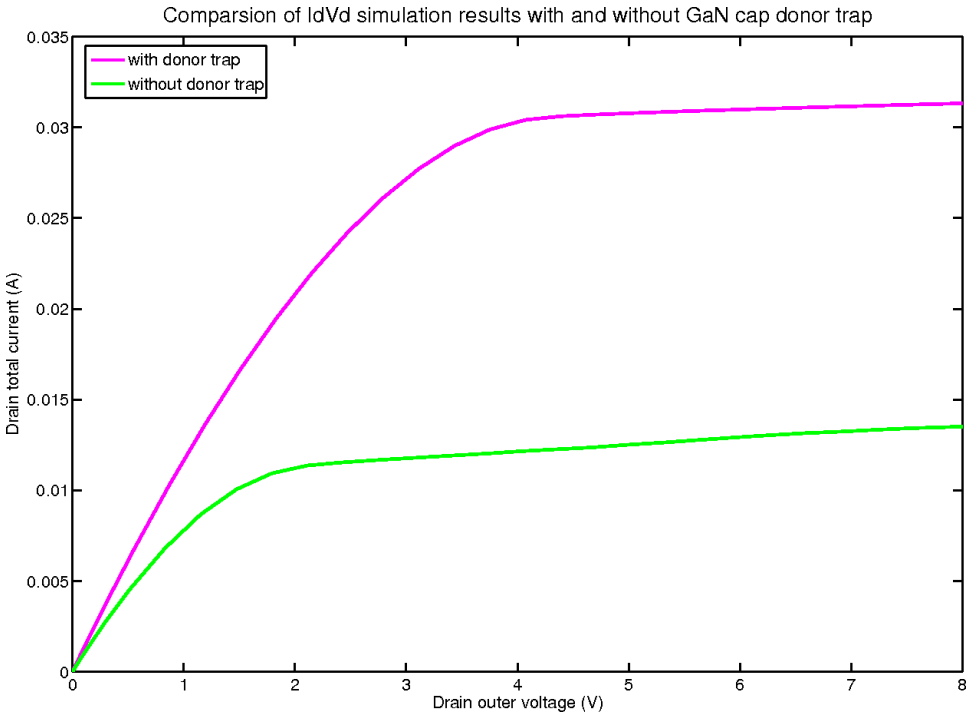

Figure 3.19: Comparison of $I_d - V_d$ simulation results with and without donor trap.

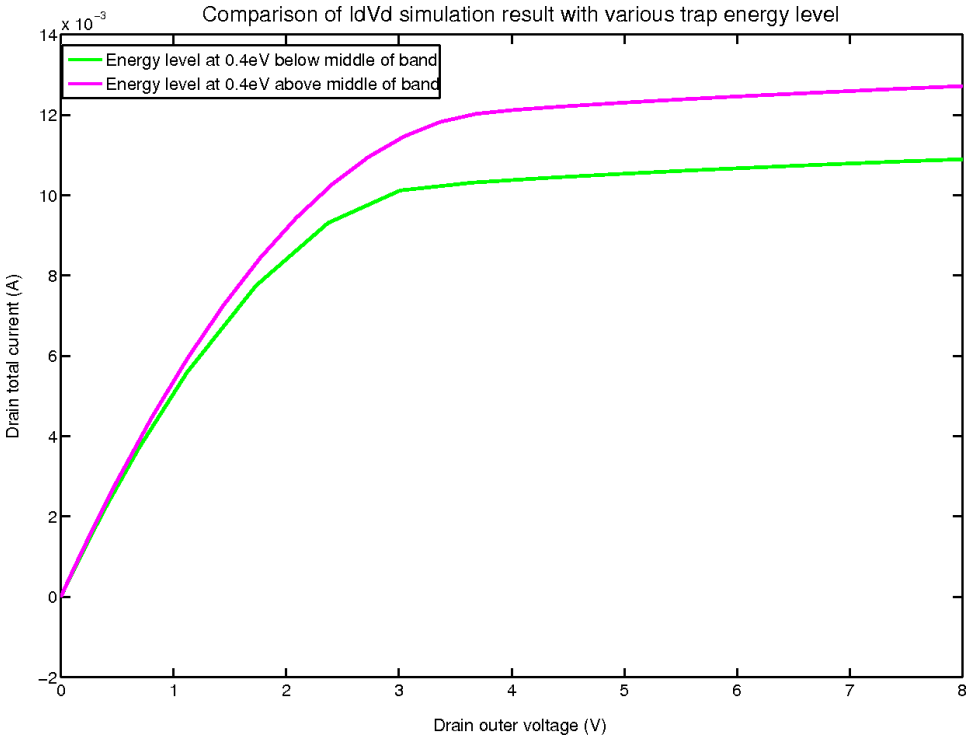

Figure 3.20: Comparison of $I_d - V_d$ simulation results with trap of various energy levels.

3.3 Simulation result matching measurement

In the following part, matching and calibration are mostly done between the simulation results and measurements. Measurement of $I_d - V_g$ curve is from device marked as Sample A while I_dV_d measurement is from device marked as Sample B.

To start with, $I_d - V_g$ simulation results are calibrated to fit measurement because once $I_d - V_g$ curves are matched, threshold voltage can be determined. The electron mobility used is 850 $cm^2/V \cdot s^{-1}$ which is the default value of simulator. The affinity of GaN is 4.1 eV and workfunction function for the gate contact Ni ranges from 5.04 eV to 5.35 eV. Thus, the approximate barrier height between GaN cap and Ni gate is 1.0 eV to 1.3 eV. Sentaurus Workbench is constructed with various barrier heights from 1.0 eV to 3.0 eV increasing with a step of 0.5 eV. The comparison of measurement of simulation results is shown in Figure 3.21. From Figure 3.21, it can be observed that simulation result from barrier height of 2.0 eV matches with measurement in threshold voltage. Thus for $I_d - V_g$ curve fitting, barrier height is adjusted to 2.0 eV. Electron mobility is adjusted to 1500 $cm^2/V \cdot s^{-1}$ to fit with measurement. Comparison of measurement and simulation result with barrier height being 2.0 eV and electron mobility being 1500 $cm^2/V \cdot s^{-1}$ is shown in Figure3.22

Figure 3.22 shows a comparison between measurement and simulation of $I_d - V_g$. Figure 3.23 shows comparison between measured transconductance g_m and simulated g_m. Presented in Figure 3.22, HEMT is turned on at around V_g = -2.0V.

Figure 3.24 shows the simulation result matching with the measurement data from device marked as Sample B which shows typical DC characteristics of HEMT. In this calibration work, barrier height of gate contact is 1.5 eV. As demonstrated in convergence control subsection, non local mesh is applied to source and drain contacts for the goal of using Schottky contact with tunneling current to replace Ohmic contact which causes convergence problem. Effective masses of AlN and GaN at contacts are modified to small value to achieve zero resistance. To start with, the effective mass is adjusted to 0.01 m_0 to reach almost zero resistance at the drain and source contacts. Electron mobility is adjusted from default value

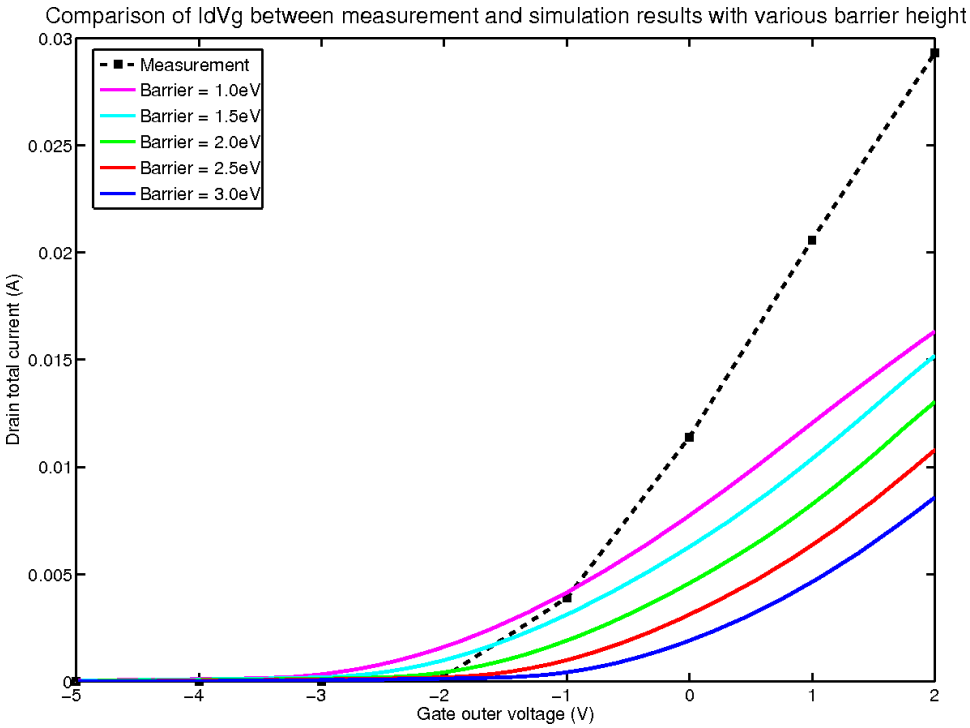

Figure 3.21: Comparison of $I_d - V_g$ measurement from sample A and simulation results with various barrier heights.

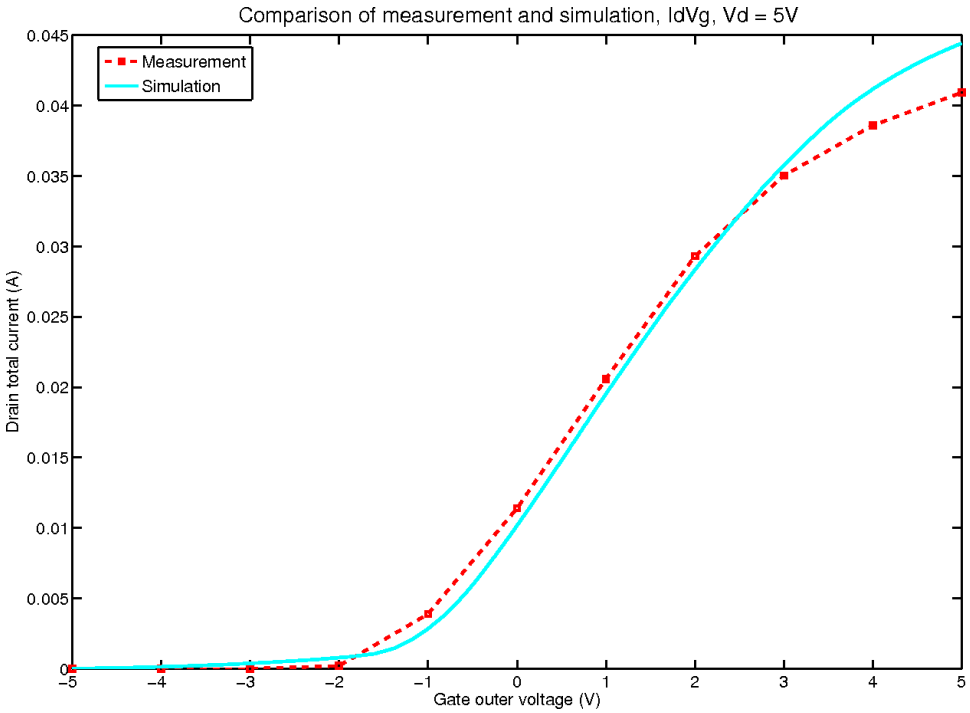

Figure 3.22: $I_d - V_g$ measurement of sample A compared with simulation.

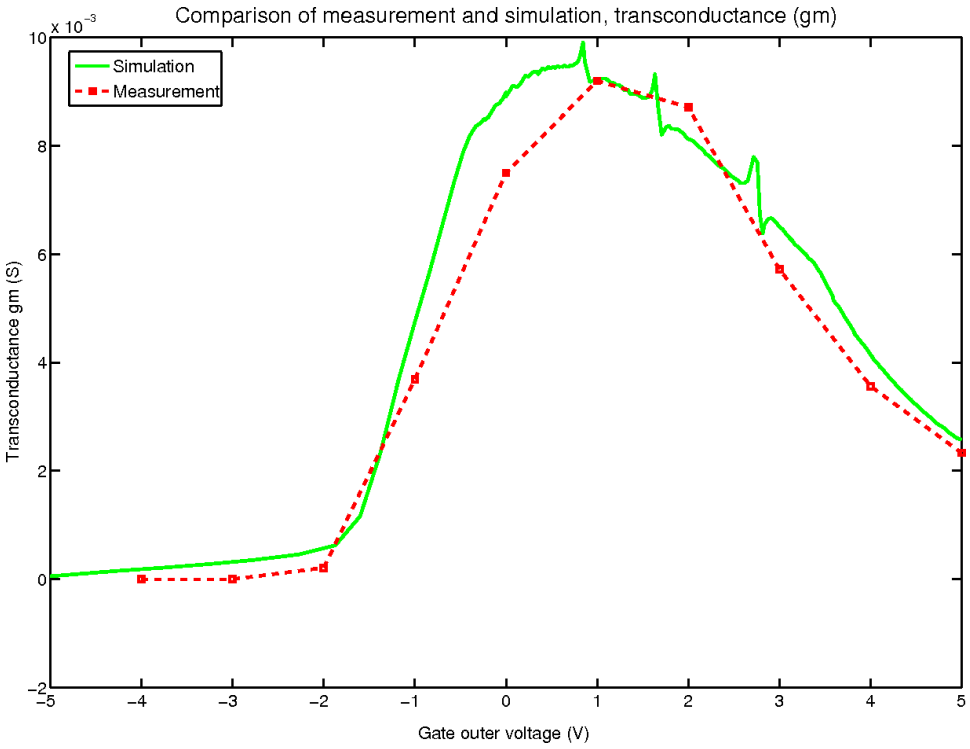

Figure 3.23: Transconductance g_m measurement of sample A compared with simulation.

850 $cm^2/V{\cdot}s^{-1}$ to 800 $cm^2/V{\cdot}s^{-1}$ to fit the measurement. Donor trap of concentration of $3{\cdot}10^{13}$ cm^{-2} with energy level locating at the middle of energy band. N-type doping of concentration of 10^{15} cm^{-3} is applied to the GaN cap and AlGaN barrier layer as the electron source of 2DEG. P-type dopant of concentration of 10^{15} cm^{-3} is applied to the GaN buffer region to reduce off-state leakage current.

To match measurement in linear region, resistance needs to be series to source and drain contacts. One way to add resistance to contact is to directly add resistance to the source and drain contact. In this work, instead of adding series resistance to contact, the effective masses of GaN and AlN at nonlocal mesh region at drain and source contacts are modified from 0.01 m_0 to 0.1 m_0 to achieve same effect. The simulation result of $I_d - V_d$ with effective mass being adjusted to 0.1 m_0 is illustrated in Figure 3.25. From Figure 3.25, it can be observed that a better match in linear region is achieved by modifying tunneling effective masses of GaN and AlN in nonlocal mesh region with tunneling contact model.

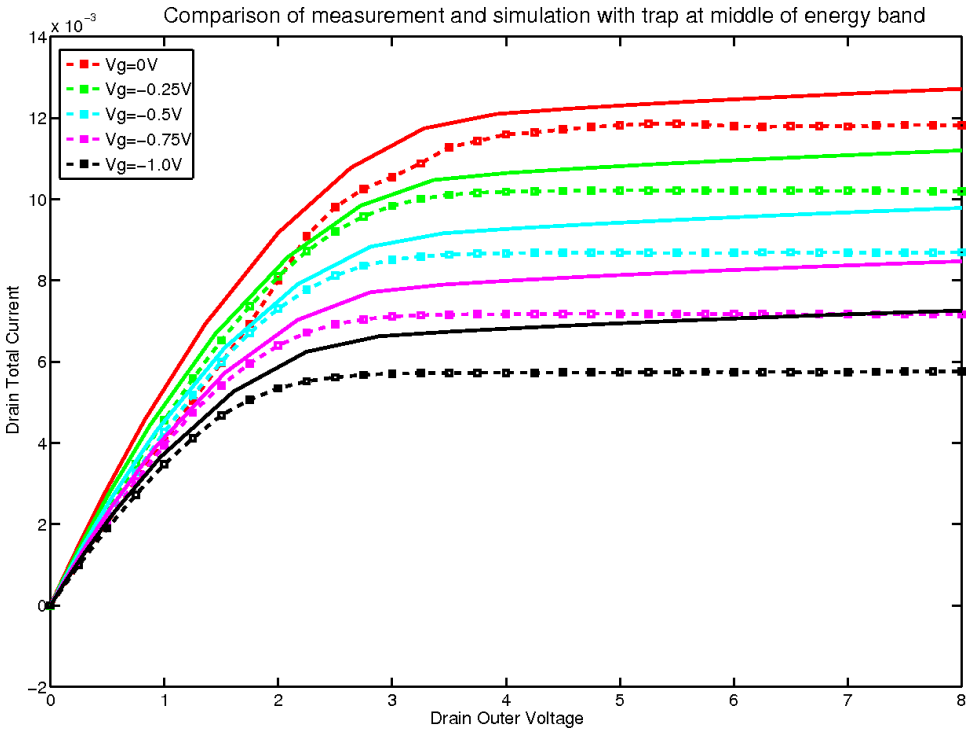

Figure 3.24: Comparison of $I_d - V_d$ measurement and simulation in tunneling contact model $m_t = 0.01\ m_0$.

This modification of effective masses only controls tunneling current of tunneling contacts but has nothing to do with effective masses of GaN and AlN in AlGaN barrier, GaN cap and GaN bulk which determine values of N_C, N_V and so on.

3.4 Gate scaling

The main goal of dimensional gate scaling is to integrate more transistors in the same area without degrading performance of single transistor. Effectively scaling gate length will lead to an increment of functionality in the same area. Gate scaling is performed in rectangular and cylindrical coordinates. With gate scaling, the electric field within the channel layer increases. An increment in current proportional to $\frac{W}{L}$ is expected for long channel device behavior. One of the goal of this work is to simulate the characteristics of the devices when gates are shrunk down to 10 um and 1 um.

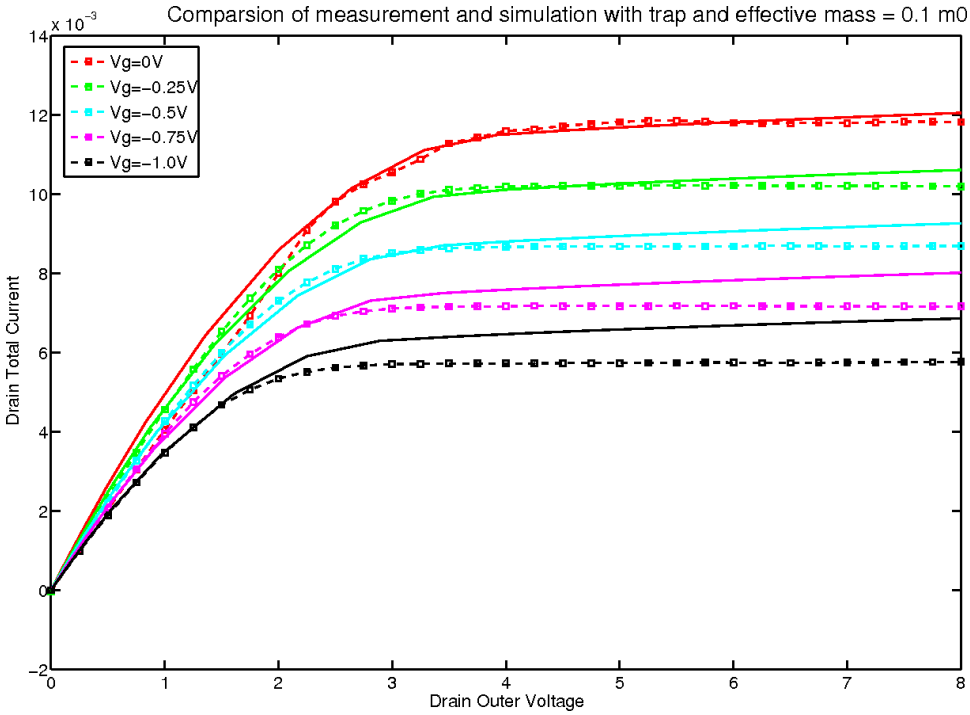

Figure 3.25: Comparison of $I_d - V_d$ measurement and simulation in tunneling contact model $m_t = 0.1\ m_0$.

Simulation results of gate scaling in rectangular coordinate are shown in Figure 3.26, Figure 3.27 and Figure 3.28. Figure 3.26 shows the comparison of simulation results when gate length is 40 um. Figure 3.27 shows the comparison of simulation results when gate length is shrunk from 40 um to 10 um. Figure 3.28 shows the comparison of simulation results when gate length is shrunk from 40 um to 1 um. When gate length is shrunk, electric field in channel will be increased since the same voltage bias is applied to the drain contact which will lead to increment in drain current density. In both Figure 3.27 and Figure 3.28 enormous increments in drain current density are observed compared with Figure 3.26.

Though significance and emphasis are drawn to the importance of gate scaling, obstacles occur due to the device size reduction. When gate length is scaled, the shrunk gate has weaker control over 2DEG in channel region. A threshold voltage shift will be observed as the result of the increasing influence of drain voltage over the shape of channel region. Threshold voltage will be a function of both gate bias and drain to source voltage. Gate

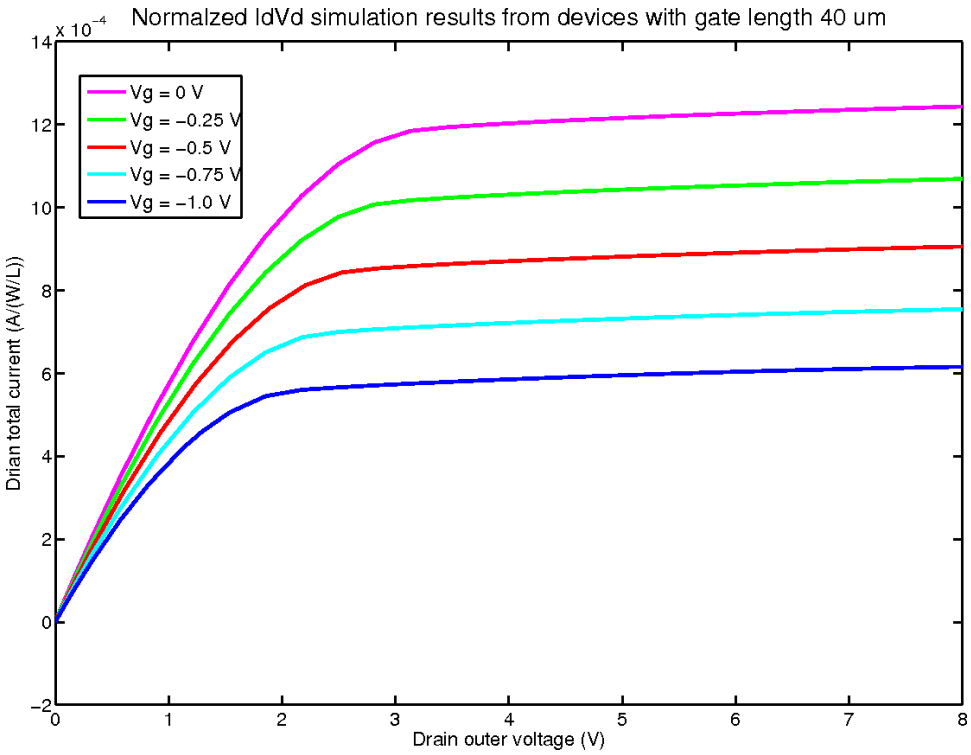

Figure 3.26: $I_d - V_d$ simulations with gate length equaling 40 um.

scaling will as well increase HEMT transconductance and off-state current. To verify the scenario, structures with gate length being shrunk down to 10 um and 1um are constructed. Schematics of HEMTs with gate length 10 um and 1 um are shown in Figure 3.29 and Figure 3.30 respectively.

During each individual gate length, drain contact is biased at 5 V and gate bias is swept from -5 V to 5 V. As gate length is further scaled, the positive drain voltage will be more influential on the charge in channel which will further lead to threshold voltage shifting to be a larger negative value. Additionally, off-state current and transconductance will increase as gate length being shrunk down to smaller value.

Comparison of $I_d - V_g$ curves with HEMT gate length being shrunk down from 40 um to 1 um is shown in Figure 3.31, while the normalized corresponding curves are shown in Figure 3.32. As gate length decreasing, drain total current increases due to the increment of electric field within the channel. When gate length reaches 1 um, short channel effect

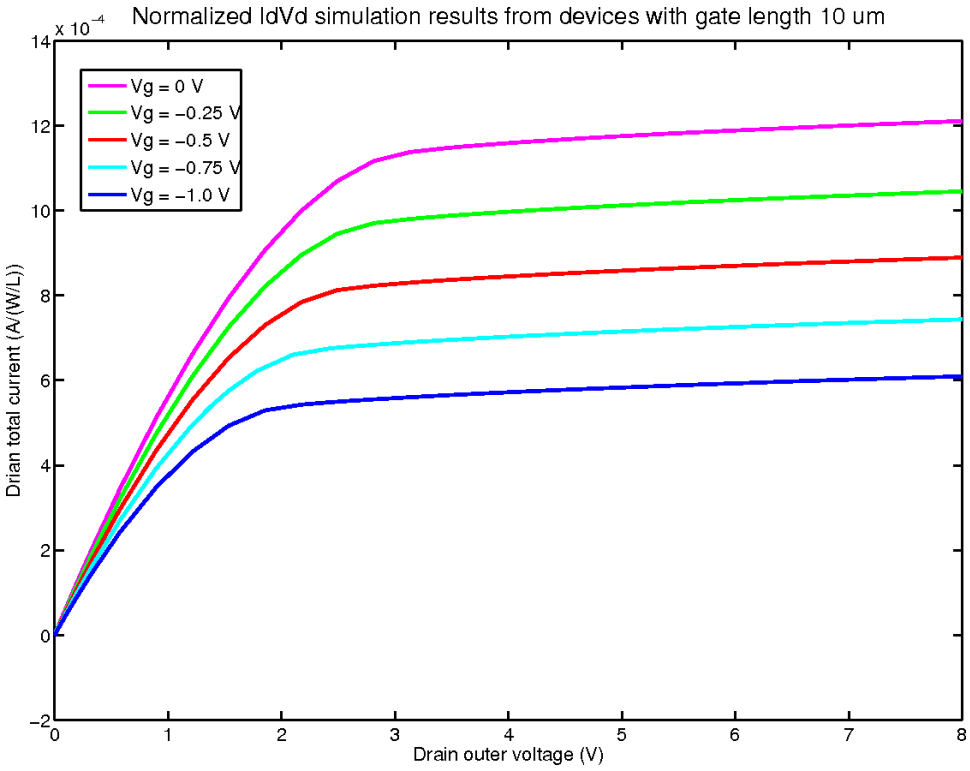

Figure 3.27: $I_d - V_d$ simulations with gate length equaling 10 um.

starts to occur. Increment in drain current does not follow the ratio of $\frac{W}{L}$ strictly due to velocity saturation. The simulation result of off-state current and transconductance as a function of gate length are shown in Figure 3.33 and Figure 3.34 respectively. In Figure 3.33 increment in off-state leakage current can be observed as the result of reduction in gate length. Moreover, Figure 3.34 indicates an obvious increment in transconductance as gate length is shrunk down from 40 um to 0.1 um.

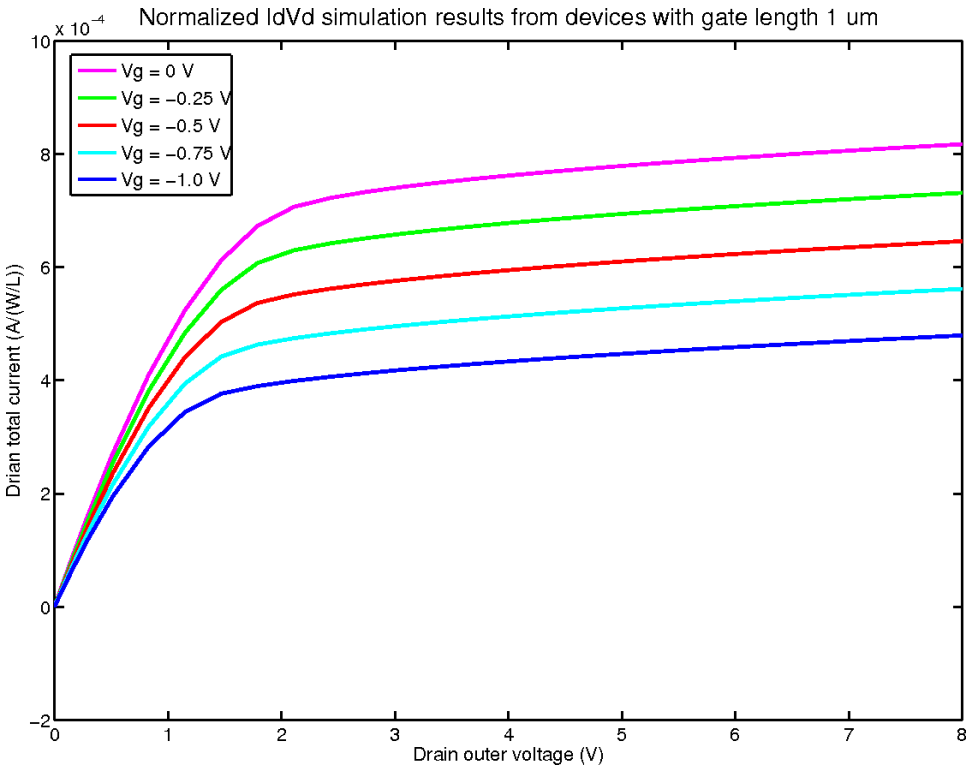

Figure 3.28: $I_d - V_d$ simulations with gate length equaling 1 um.

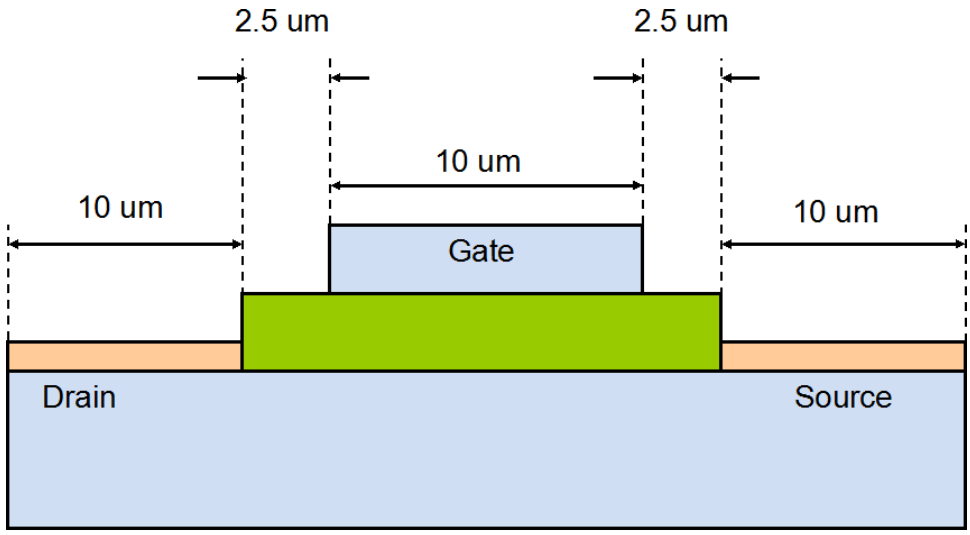

Figure 3.29: Schematic of HEMT with gate length being shrunk to 10 um.

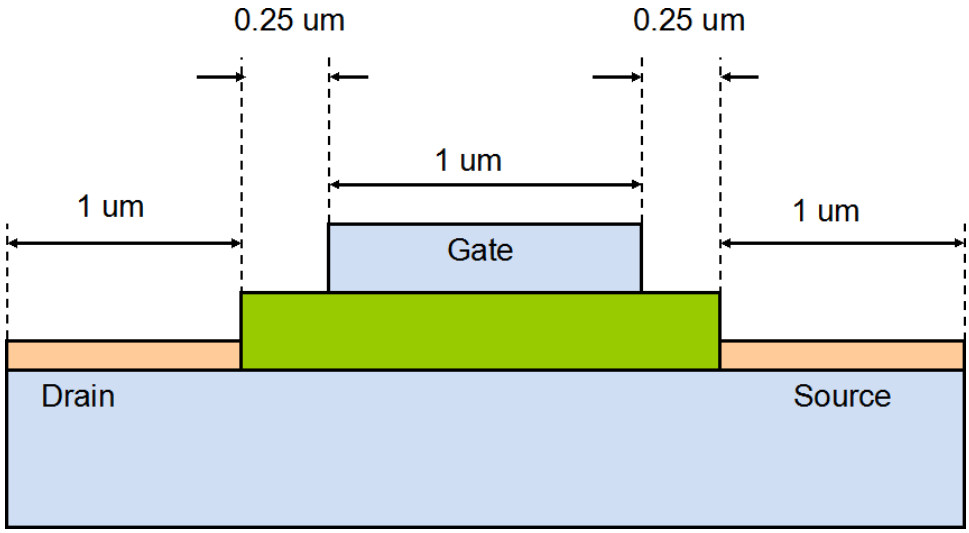

Figure 3.30: Schematic of HEMT with gate length being shrunk to 1 um.

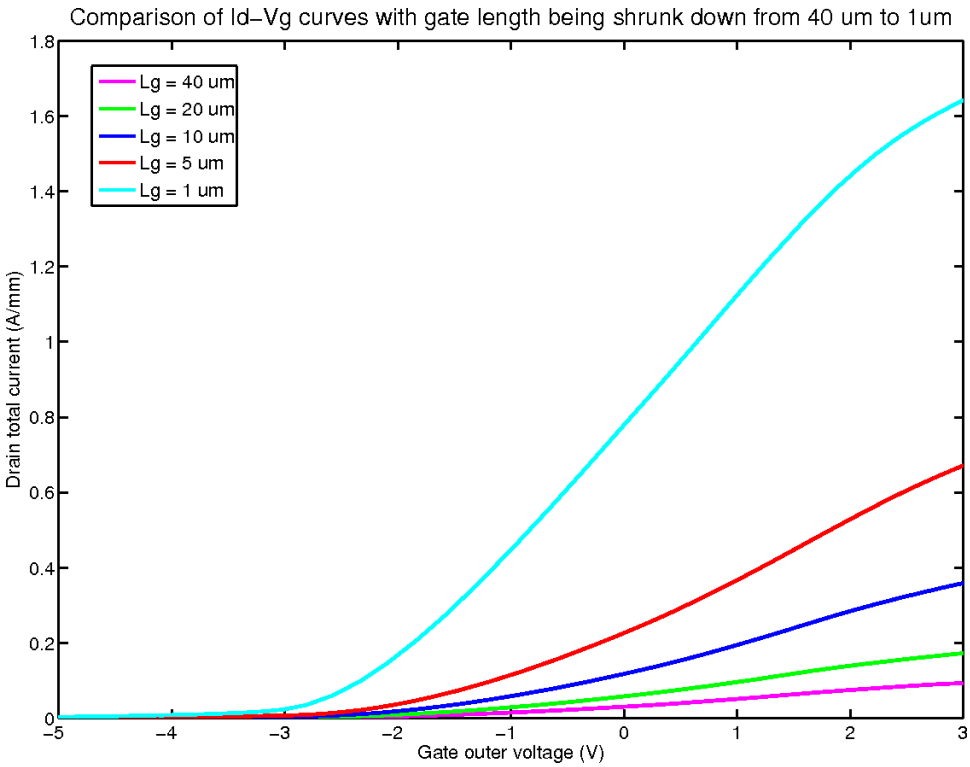

Figure 3.31: Comparison of $I_d - V_g$ from HEMTs with gate length being shrunk down from 40 um to 1 um.

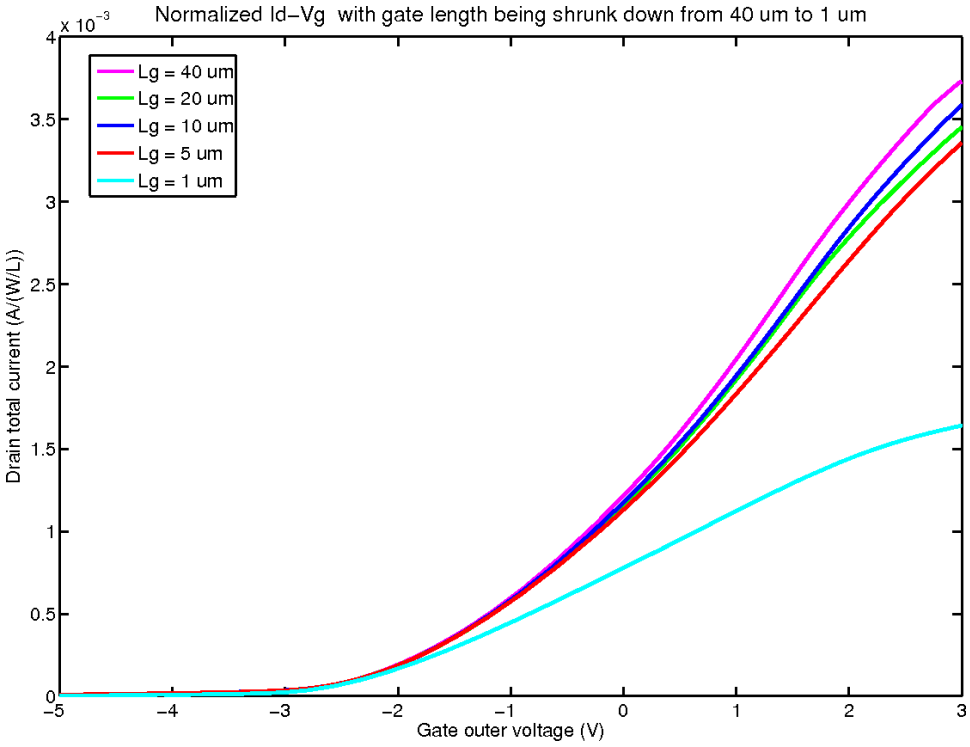

Figure 3.32: Comparison of normalized $I_d - V_g$ from HEMTs with gate length being shrunk down from 40 um to 1 um.

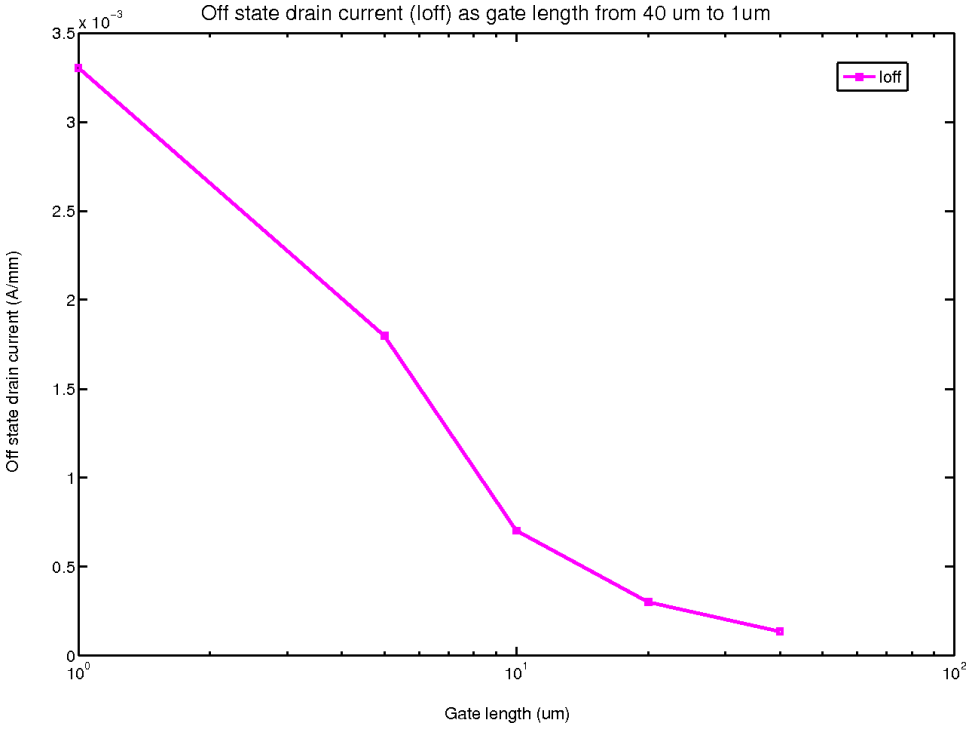

Figure 3.33: Off state drain current density as gate length shrunk from 40 um to 1 um.

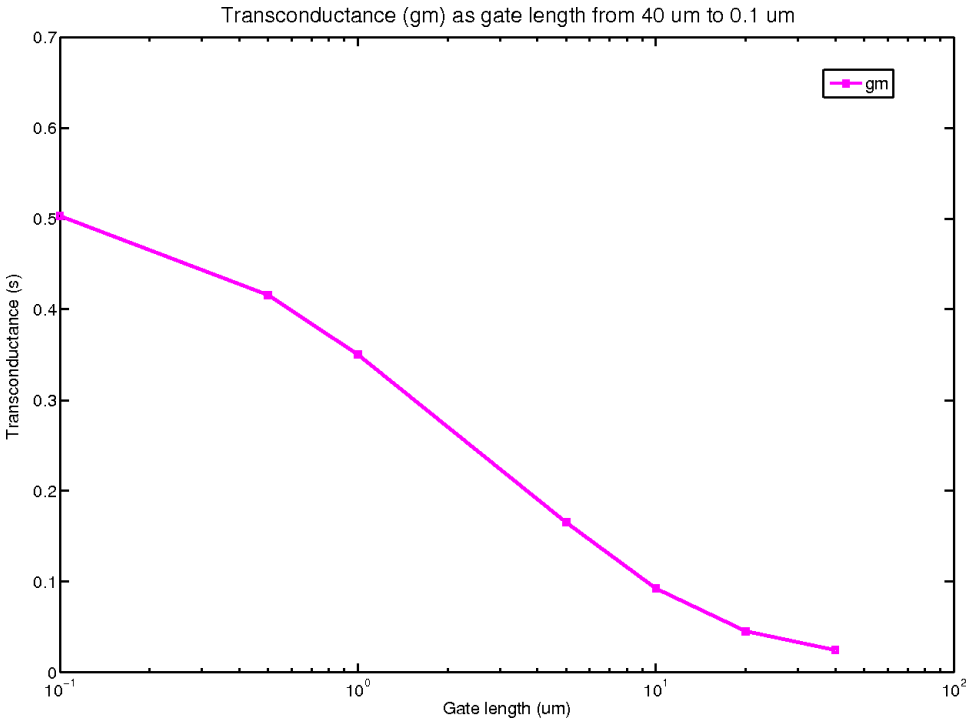

Figure 3.34: Transconductance as gate length shrunk from 40 um to 0.1 um.

Chapter 4

Conclusion and future work

TCAD has been used to simulate and match measured I-V characteristics for a GaN based HEMT. Many issues are carefully taken into consideration such as: the thickness of AlGaN barrier, the doping concentration of GaN buffer, the Al mole concentration of barrier layer, the electron mobility and the model used for polarization charge density calculation. Moreover, series contact resistance is adjusted through the electron barrier tunneling model provided by the simulator. Furthermore, for the goal of reducing un-gated region resistance and achieving charge modulation in 2DEG, donor trap of concentration $5{\cdot}10^{13}\ cm^{-2}$, energy level locating at 0.4 eV below middle of energy band is applied to the un-gate region at GaN/Nitride interface. Finally, gate scaling is performed on the manual charge placement HEMT in rectangular coordinate. Improvement of drain current density is observed as gate length being shrunk down. However, shift in threshold voltage, increment in transconductance and off-state current also occur as the drawback of gate length scaling.

In the future work, I would like to emphasize the effect of trap on the performance of GaN HEMT. A more detail simulation includes but not limits DC simulation, RF simulation and transient simulation will be constructed to explore the influence of trap in affecting reliability.

Bibliography

[1] De Brida Christian, Gallium Nitride simulations using Sentaurus software, University of Padova, Department of Information Engineering, Dec. 2010.

[2] Slack. G., Nonmetallic crystals with high thermal conductivity, *Journal of Physics and Chemistry of Solids*, Vol. 34, No. 2, PP. 321-335, 1973.

[3] Young Chul Choi, Milan Pophristic, Ho-Young Cha, Boris Peres, Michael G. Spencer, and Lester F.Eastman. The effect of an Fe-doped GaN buffer on off-state breakdown characteristics in AlGaN/GaN HEMTs on Si substrate. *Electron Devices, IEEE transaction*, Vol. 53, No. 12, PP. 2926-2931, Dec. 2006.

[4] I. P. Smorchkova, C. R. Elsass, J. P. Ibbetson and R. Vetury, B. Heying, P. Fini and E. Haus, S. P. DenBaars. Polarization-induced charge and electron mobility in AlGaN/GaN heterostructures grown by plasma-assisted molecular-beam epitaxy. *Journal of Applied Physics*, Vol. 86, No. 8, PP. 4520-4526, Oct. 1999.

[5] J. P. Ibbtson, P. T. Fini, K. D. Ness, S. P. DenBaars, J. S. Speck and U. K. Mishra, Polarization effect, surface states, and the source of electrons in AlGaN/GaN heterostructure field effect transistors, *Journal of Applied Physics*, Vol. 77, No. 2, PP. 250-252, July 2000.

[6] O. Hartin, Bruce Green, AlGaN/GaN HEMT TCAD Simulation and Model Extraction for RF Application, Freescale, Tempe, AZ 2100 E. Elliot/85284, USA, *Bipolar/BiCMOS Circuits and Technology Meeting (BCTM), IEEE*, PP. 232-236, Oct. 2010.

[7] P. M. Asbeck, E. T. Yu, S. S. Lau, G. J. Sullivan, J. Van Hove, and J. Redwing, Piezoelectric charge density in AlGaN/GaN HFETs, *Electron Letters*, Vol. 33, No. 14, PP. 1230-1231, Jul. 1997.

[8] S. Keller, G. Parish, P. T. Fini, S. Heikman, C. H. Chen, N. Zhang, S. P. DenBaars, U. K. Mishra, and Y. F. Wu, Metal organic chemical vapor deposition of high mobility AlGaN/GaN heterostructures *Journal of Applied Physics*, Vol. 86, No. 10, PP. 5850-5857, Nov. 1999.

[9] O. Ambacher, J. Smart, J. R. Shealy, N. G. Weimann, K. Chu, M. Murphy, W. J. Schaff, and L. F. Eastman, Two-dimensional electron gases induced by spontaneous and piezoelectric polarization charges in N-face and G-face AlGaN/GaN heterostructures, *Journal of Applied Physics*, Vol. 87, No. 1, PP. 334-344, Jan. 2000.

[10] Ashwing Ashok, Dragica Vasileska, Senior Member, IEEE, Stephen M. Goodnick, Fellow, IEEE, and Olin Hartin, Importance of the gate-dependent polarization charge on the operation of GaN HEMTs, *IEEE Transactions on Electron Eevices*, Vol.56 No. 5, PP.998-1006, May 2009.

[11] L. Hsu and W. Walukiewicz, Effects of piezoelectric field on defect formation, charge transfer, and electron transport at $GaN/Al_xGa_{1-x}N$ interfaces,*Applied Physics Letter*, Vol. 73, No. 3, July 1998.

[12] M. C. J. C. M. Krmer, Gallium Nitride-based Microwave High-Power Heterojunction Field-Effect Transistors, design, technology, and characterization, Eindhoven University of Technology, 2006.

[13] S. J. Pearton, J. C. Zolper, R. J. Shul, and F. Ren, GaN: Processing, defects, and devices, *Journal of Applied Physics*, Vol. 86, No. 1, PP. 1-78, July 1999.

[14] Aditya Kalavagunta, Understanding the impact of bulk traps on GaN HEMT DC and RF characteristics, University of Vanderbilt, May 2009.

[15] P. K. Klein and S. C. Binari, Photoionization spectrocopy in AlGaN/GaN high electron mobility transistors grown by molecular beam epitaxy, *Journal of Applied Physics*, Vol. 92, No. 9, PP. 5498-5502, Nov. 2002.

[16] P. K. Klein and S. C. Binari, Photoionization spectrocopy of deep defects responsible for current collapse in nitride-based field effect transistors, *Journal of Physics: Condensed Matter*, Vol. 15, No. 44, PP. 1647-1661, Nov. 2003.

[17] P. K. Klein and S. C. Binari, J. A. Freitas, and A. E. Wickenden, Photoionization spectrocopy of traps in GaN metal-semiconductor field-effect transistors, *Journal of Applied Physics*, Vol. 88, No. 5, PP. 2843-2852, Sept. 2000.

[18] P. K. Klein and S. C. Binari, J. A. Freitas, and A. E. Wickenden, Observation of deep traps responsible for current collapse in GaN metal-semiconductor field effect transistors, *Applied Physics Letters*, Vol. 75, No. 25, PP. 4016-4018, Dec. 1999.

[19] Elias W. Faraclas, A. F. M. Anwar, AlGaN/GaN HEMTs: Experiment and simulation of DC characteristics, *Solid State Electronics*, Vol. 50, No. 6, PP. 2051-2056, June 2006.

[20] A. Tarakji, G. Simin, N. Ilinskaya, X. Hu, A. Kumar, A. Koudymov, J. Yang, M. A. Khan, M. S. Shur, and R. Gaska, Mechanism of radio-frequency current collapse in GaN-AlGaN field-effect transistors, *Applied Physics Letters*, Vol. 78 No. 15, PP. 2169-2172, Apr. 2001.

[21] T. Mizutani, Y. Ohno, M. Akita, S. Kishimoto, and K. Maezawa, A study on current collapse in AlGaN/GaN HEMTs induced by bias stress, *IEEE transactions on Electron Devices*, Vol. 50, No. 10, PP. 2015-2020, Oct. 2003.

[22] R. Vetury, N. Q. Q. Zhang, S. Keller, and U. K. Mishra, The impact of surface states on the DC and RF characteritics of AlGaN/GaN HFETs, *IEEE transactions on Electron Devices*, Vol. 48, No. 3, PP. 560-566, Mar. 2001.

[23] Jungwoo Joh and Jesus A. del Alamo, Mechanisms for electrical degradation of GaN high-electron mobility transistors, *Electron Devices Meeting, 2006. IEDM 06 International*, PP. 1-4, Dec. 2006.

[24] J.A. del Alamo and J. Joh. GaN HEMT reliability. *Microelectronics Reliability*, Vol. 49, PP. 1200-1206, July 2009

[25] J. W. Johnson, J. Han, A. G. Baca, R. D. Briggs, R. J. Shul, J. R. Wendt, C. Monier, F. Ren, B. Luo, S. N. G. Chu, D. Tsvetkov, V. Dmitriev, and S. J. Pearton, Comparison of AlGaN/GaN high electron mobility transistors grown on AlN/SiC templates or sapphire, *Solid State Electronics*, Vol .46, No. 4, PP. 513-523, Apr. 2002.

[26] P. B. Klein, S. C. Binari, K. Ikossi-Anastasiou, A. E. Wickenden, D. D. Koleske, R. L. Henry, and D. S. Katzer, Investigation of traps producing current collapse in AlGaN/GaN high electron mobility transistors, *Electronics Letters*, Vol. 37, No. 10, PP. 661-662, May 2001.

[27] Sentaurus Device, Synopsis Inc. Version 2012.09.